Milan J. Math. Vol. 79 (2011) 597–642
DOI 10.1007/s00032-011-0171-6
Published online November 4, 2011

Milan Journal of Mathematics

Phase Field Approach to Multiphase Flow Modeling

Andrea G. Lamorgese, Dafne Molin and Roberto Mauri

Abstract. We review the phase field (otherwise called diffuse interface) model for fluid flows, where all quantities, such as density and composition, are assumed to vary continuously in space. This approach is the natural extension of van der Waals' theory of critical phenomena both for one-component, two-phase fluids and for partially miscible liquid mixtures. The equations of motion are derived, assuming a simple expression for the pairwise interaction potential. In particular, we see that a non-equilibrium, reversible body force appears in the Navier-Stokes equation, that is proportional to the gradient of the generalized chemical potential. This, so called Korteweg, force is responsible for the convection that is observed in otherwise quiescent systems during phase change. In addition, in binary mixtures, the diffusive flux is modeled using a Cahn-Hilliard constitutive law with a composition-dependent diffusivity, showing that it reduces to Fick's law in the dilute limit case. Finally, the results of several numerical simulations are described, modeling, in particular, a) mixing, b) spinodal decomposition, c) nucleation, d) enhanced heat transport, e) liquid-vapor phase separation.

Mathematics Subject Classification (2010). Primary 82C26; Secondary 76T99.

Keywords. Dynamic phase transitions, phase field model, multiphase flows.

1. Introduction

The theory of multiphase systems was developed at the beginning of the 19th century by Young, Laplace and Gauss, assuming that different phases are separated by an interface, that is a surface of zero thickness. In this approach, physical properties such as density and concentration, may change discontinuously across the interface and the magnitude of these jumps can be determined by imposing equilibrium conditions at the interface. For example, imposing that the sum of all forces applied to an infinitesimal curved interface vanish leads to the Young-Laplace equation, stating that the difference in pressure between the two sides of the interface (where each phase is assumed to be at equilibrium) equals the product of surface tension and

curvature. Later, this approach was generalized by defining surface thermodynamical properties, such as surface energy and entropy, and surface transport quantities, such as surface viscosity and heat conductivity, thus formulating the thermodynamics and transport phenomena of multiphase systems. At the end of the 19th century, though, another approach was proposed by Rayleigh [49] and Van der Waals [59], who assumed that interfaces have a non-zero thickness, i.e. they are "diffuse." Actually, the basic idea was not new, as it dated back to Maxwell [37] and Gibbs [15], Poisson [48] and Leibnitz [33] or even Lucretius [35], who wrote that "a body is never wholly full nor void." Concretely, in a seminal article published in 1893, Van der Waals [59] used his equation of state to predict the thickness of the interface, showing that it becomes infinite as the critical point is approached. Later, Korteweg [25] continued this work and proposed an expression for the capillary stresses, which are generally referred to as Korteweg stresses, showing that they reduce to surface tension when the region where density changes from one to the other equilibrium value collapses into a sharp interface (see [51] for a review of the molecular basis of capillarity).

In the first half of the 20th century, van der Waals' theory of critical phenomena was generalized by Ginzburg and Landau [31], leading to a general theory of second-order phase transition and thereby describing phenomena such as ferromagnetism, superfluidity and superconductivity. Then, at mid 1900, Cahn & Hilliard [6] applied van der Waals' diffuse interface (D.I.) approach to binary mixtures and then used it to describe nucleation and spinodal decomposition [3]. This approach was later extended to model phase separation of polymer blends and alloys [11]. Finally, in the mid 1970s, the D.I. approach was coupled to hydrodynamics, developing a set of conservation equations, thanks to the work by, among others, Kawasaki [24], Siggia [55], and Hohenberg & Halperin [20]. These latter authors referred to this approach as "model H" and only later the name "diffuse interface model" was introduced. Finally, recent developments in computing technology have stimulated a resurgence of the D.I. approach, above all in the study of systems with complex morphologies and topological changes. A detailed discussion about D.I. theory coupled with hydrodynamics can be found in Antanovskii [2], Lowengrub & Truskinovski [34], Anderson *et al.* [1] and, more recently, in Onuki [34] and Thiele *et al.* [58]. In order to better understand the basic idea underlying the D.I. theory, let us remind briefly the classical approach to multiphase flow that is used in fluid mechanics. There, the equations of conservation of mass, momentum, energy and chemical species are written separately for each phase, assuming that temperature, pressure, density and composition of each phase are equal to their equilibrium values. Accordingly, these equations are supplemented by boundary conditions at the interface, namely [9],

$$\|\boldsymbol{\tau}\|_+^- \cdot \mathbf{n} = \kappa\sigma\mathbf{n} - (\mathbf{I} - \mathbf{nn}) \cdot \nabla\sigma, \qquad \|\mathbf{v}\|_+^- = 0, \qquad \|T\|_+^- = 0, \tag{1.1}$$

with $\mathbf{n}$ denoting the normal at the interface, stating that the jump of the stress tensor, $\boldsymbol{\tau}$, at the interface is related to the the curvature κ, the surface tension σ and its gradient, while the velocity $\mathbf{v}$ and the temperature T are continuous. Similar

boundary conditions exist also for the transport of energy and mass,

$$\|\mathbf{J_q}\|_+^- \cdot \mathbf{n} = 0, \qquad \|\mathbf{J}^{(i)}\|_+^- \cdot \mathbf{n} = 0, \qquad \|\rho^{(i)}\|_+^- = (K-1)\rho^{(i)+}, \tag{1.2}$$

stating that standard (Fourier) heat flux, $\mathbf{J_q}$, and the diffusive flux of any chemical species i, $\mathbf{J}^{(i)}$, are continuous across the interface (assuming no phase transition and no surface reactions), while the concentration, $\rho^{(i)}$, can undergo a jump, depending on a partition coefficient K, given by thermodynamics. Naturally, this results in a free boundary problem, which means that one of the main problems of this approach is to determine the position of the interface. To that extent, many interface tracking methods have been developed, which have proved very successful in a wide range of situations. However, interface tracking breaks down whenever the interface thickness is comparable to the length scale of the phenomenon that is being studied, such as a) in near-critical fluids or partially miscible mixtures, as the interface thickness diverges at the critical point, and the morphology of the systems presents self-intersecting free boundaries; b) near the contact line along a solid surface, in the breakup/coalescence of liquid droplets and, in general, in microfluidics, as the related physical processes act on length scales that are comparable to the interface thickness. In front of these difficulties, the D.I. method offers an alternative approach. Quantities that in the free boundary approach are localized in the interfacial surface, here are assumed to be distributed within the interfacial volume. For example, surface tension is the result of distributed stresses within the interfacial region, which are often called capillary, or Korteweg, stresses. In general, the interphase boundaries are considered as mesoscopic structures, so that any material property varies smoothly at macroscopic distances along the interface, while the gradients in the normal direction are steep. Accordingly, the main characteristic of the D.I. method is the use of an "order parameter" which undergoes a rapid but continuous variation across the interphase boundary, while it varies smoothly in each bulk phase, where it can even assume constant equilibrium values. For a single-component system, the order parameter is the fluid density ρ, for a liquid binary mixture it is the molar (or mass) fraction ϕ, while in other cases it can be any other parameter, not necessarily with any physical meaning, that allows to reformulate free boundary problems. In all these cases, the D.I. model must include a characteristic interface thickness, over which the order parameter changes. In fact, in the asymptotic limit of vanishing interfacial width, the diffuse interface model reduces to the classical free boundary problem.

In this work, first, in Section 2 and 3, the diffuse interface model is formulated for single-component fluids at equilibrium. Then, in Section 4, the equations of motion are developed both for for single- and multi-component fluid mixtures, while in Section 5, these results are applied to regular binary mixtures. Finally, after a brief summary of all the equations of motion (Section 6), in Section 7, the results of numerical simulations are presented for the case of regular liquid binary mixtures and single-component van der Waals fluids.

2. Equilibrium conditions for single-component fluids

2.1. The free energy and van der Waals' equation

All thermodynamical properties can be determined from the Helmholtz free energy. This, in turn, depends on the intermolecular forces which, in a dense fluid, are a combination of weak and strong forces. Fortunately, strong interactions nearly balance each other, so that the net forces acting on each molecule are weak and long-range. In addition, the mean field approximation is assumed to be applicable, meaning that molecular interactions are smeared out and can be replaced by the action of a continuous effective medium [43]. Based on these assumptions, the case of dense fluids can be treated as that of nearly ideal gases, so that, allowing for variable density, the specific (per unit mass) Helmholtz free energy at constant temperature T can be written as (see Landau & Lifshitz [31], Ch. 74):

$$f[\rho(\mathbf{x})] = f_{id} + \frac{1}{2}\frac{kT}{m^2}\int \left(1 - e^{-U(r)/kT}\right)\rho(\mathbf{x}+\mathbf{r})\, d^3\mathbf{r}, \tag{2.1}$$

where k is Boltzmann's constant, m is the mass of each molecule, U is the pair interaction potential, which depends on the distance $r = |\mathbf{r}|$, ρ is the mass density, while the factor $1/2$ compensates counting twice the interacting molecules. The first term on the RHS,

$$f_{id} = \frac{kT}{m}\ln\rho, \tag{2.2}$$

is the specific free energy of an ideal gas (where molecules do not interact). Now, we assume that the interaction potential consists of a long-range attractive term, decaying as r^{-6} (like in the Lennard-Jones potential), while the short-range term is replaced by a hard-core repulsion [21], i.e.,

$$U(r) = \begin{cases} -U_0(\ell/r)^6 & (r > d) \\ \infty & (r < d) \end{cases} \tag{2.3}$$

where d is the nominal hard-core molecular diameter, ℓ is a typical intermolecular interaction distance, and the non-dimensional constant U_0 represents the strength of the intermolecular potential. When the density is uniform, Eq. (2.1) yields the thermodynamic specific free energy, f_{Th},

$$f_{Th}(T,\rho) = f_{id}(T,\rho) + f_{ex}(T,\rho), \tag{2.4}$$

where

$$f_{ex}(T,\rho) = \frac{kT}{m}\rho B(T) \tag{2.5}$$

is the excess (i.e. the non ideal part) of the free energy, with

$$B(T) = \frac{1}{2m}\int_0^\infty (1 - e^{-U(r)/kT})4\pi r^2\, dr \tag{2.6}$$

denoting the first virial coefficient. This integral can be solved as

$$B(T) = \frac{2\pi}{m}\int_0^d r^2 dr + \frac{2\pi}{m}\int_d^\infty (1 - e^{\frac{U_0}{kT}(\ell/r)^6})r^2\, dr = c_2 - \frac{m}{kT}c_1, \tag{2.7}$$

where

$$c_1 = \frac{2\pi}{3}\frac{U_0\ell^6}{m^2d^3} \quad \text{and} \quad c_2 = \frac{2\pi}{3}\frac{d^3}{m} \tag{2.8}$$

are the pressure adding term and the excluded specific volume, respectively. Finally we obtain:

$$f_{Th}(\rho, T) = f_{id} + \frac{kT}{m}c_2\rho - c_1\rho \approx \frac{kT}{m}\ln\left(\frac{\rho}{1-c_2\rho}\right) - c_1\rho, \tag{2.9}$$

that is,

$$f_{Th}(\rho, T) = -\frac{kT}{m}\ln(v - c_2) - \frac{c_1}{v}, \tag{2.10}$$

where $v = \rho^{-1}$ is the specific volume. At this point, applying the thermodynamic equality (see [31], Ch. 76) $P = -(\partial f/\partial v)_{N,T}$, we obtain the van der Waals' equation of state,

$$\left(P + \frac{c_1}{v^2}\right) = \frac{k}{m}\frac{T}{v - c_2}. \tag{2.11}$$

This equation of state could be considerably improved if the term $T/(v - c_2)$, which is exact in 1D, is replaced by a more accurate representation of the pressure for a hard-sphere fluid in 3D.

2.2. The critical point

In the $P-T$ diagram, the vapor-liquid equilibrium curve stops at the critical point, characterized by a critical temperature T_C and a critical pressure P_C. At higher temperatures, $T > T_C$, and pressures, $P > P_C$, the differences between liquid and vapor phases vanish altogether and we cannot even speak of two different phases. In particular, as the critical point is approached, the difference between the specific volume of the vapor phase and that of the liquid phase decreases, until it vanishes at the critical point. Accordingly, near the critical point, since the specific volumes of the two phases, v and $v + \delta v$, are near to each other, we can easily obtain:

$$\left(\frac{\partial P}{\partial v}\right)_{T_C} = 0, \quad \left(\frac{\partial^2 P}{\partial v^2}\right)_{T_C} = 0. \tag{2.12}$$

Therefore, the critical point corresponds to a horizontal inflection point in the $P - v$ diagram, which means that, since $P = -(\partial f_{Th}/\partial v)_T$,

$$\left(\frac{\partial^2 f_{Th}}{\partial v^2}\right)_{T_C} = 0, \quad \left(\frac{\partial^3 f_{Th}}{\partial v^3}\right)_{T_C} = 0. \tag{2.13}$$

Imposing that at the critical point the $P - v$ curve have a horizontal inflection point, we can determine the constant c_1 e c_2 in the van der Waals equation (the same is true for any two-parameter cubic equation of state) in terms of the critical constants T_C and P_C, finding (see [31], Ch. 84):

$$c_1 = \frac{9k}{8m}T_C v_C = \frac{27k^2}{64m^2}\frac{T_C^2}{P_C} \quad \text{and} \quad c_2 = \frac{1}{3}v_C = \frac{k}{8m}\frac{T_C}{P_C}. \tag{2.14}$$

Viceversa, the critical pressure, temperature and volume can be determined as functions of c_1 and c_2 as follows:

$$P_C = \frac{1}{27}\frac{c_1}{c_2^2}, \qquad T_C = \frac{8m}{27k}\frac{c_1}{c_2}, \qquad v_C = 3c_2. \tag{2.15}$$

Using these expressions, the van der Waals equation can be written in terms of the reduced coordinates as:

$$\left(P_r + \frac{3}{v_r^2}\right)(3v_r - 1) = 8T_r, \qquad P_r = \frac{P}{P_C}, \qquad v_r = \frac{v}{v_C}, \qquad T_r = \frac{T}{T_C}. \tag{2.16}$$

This equation represents a family of isotherms in the $P_r - v_r$ plane describing the state of any substance, which is the basis of the law of corresponding states. As expected, when $T_r > 1$ the isotherms are monotonically decreasing, in agreement with the stability condition $(\partial P/\partial v)_T < 0$, while when $T_r < 1$ each isotherm has a maximum and a minimum point and between them we have an instability interval, with $(\partial P/\partial v)_T > 0$, corresponding to the two-phase region (see Figure 1).

Note that, considering that $P_C v_C = (3k/8m)T_C$ and substituting the expressions for c_1 and c_2 in terms of the intermolecular potential, we obtain the following relation:

$$\left(\frac{\ell}{d}\right)^2 = \frac{3}{2}\left(\frac{kT_C}{U_0}\right)^{1/3}. \tag{2.17}$$

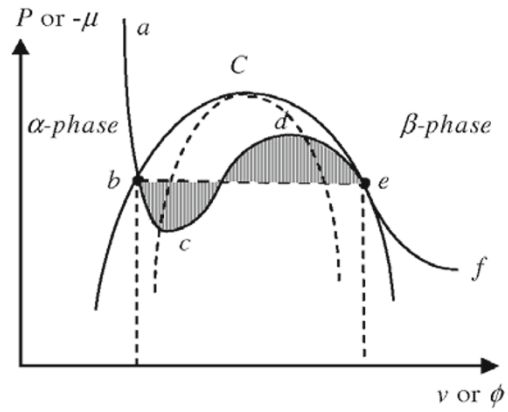

FIGURE 1. Phase diagram (P vs. v) of a single component fluid and ($-\mu_{Th}$ vs. ϕ) of a binary mixture.

2.3. Coexistence and spinodal curves

Let us consider a one-component system at equilibrium, whose pressure and temperature are below their critical values, so that it is separated into two coexisting phases, say α and β. According to the Gibbs phase rule, these two phases have the same pressure and temperature and therefore, defining the Gibbs specific free energy $g_{Th} = f_{Th} + Pv$, with $dg_{Th} = -sdT + vdP$, the corresponding equilibrium, or saturation, pressure P_{sat} at a given temperature can be easily determined from the equilibrium condition, stating that at equilibrium the Gibbs specific free energies of the two phases must be equal to each other. So we obtain:

$$g_{Th}^{\beta} - g_{Th}^{\alpha} = \int_b^e dg_{Th} = 0 \quad \Longrightarrow \quad \int_b^e v\, dP = [vP]_b^e - \int_b^e P\, dv = 0, \tag{2.18}$$

where $P = P(v)$ represents an isotherm transformation. From a geometrical point of view, this relation manifests the equality between the shaded area of Figure 1 (Maxwell's rule), where the points b and e correspond to the equilibrium, or saturation, points of the liquid and vapor phases at that temperature at equilibrium, respectively, with specific volumes v_e^{α} and v_e^{β}. Conversely, the specific volumes of the two phases at equilibrium could also be determined from the specific free energy f_{Th}, rewriting Eq. (2.16) in terms of reduced coordinates as

$$\frac{f_{Th}}{kT_C/m} = -T_r \ln(v_C) - T_r \ln\left(v_r - \frac{1}{3}\right) - \frac{9}{8v_r}. \tag{2.19}$$

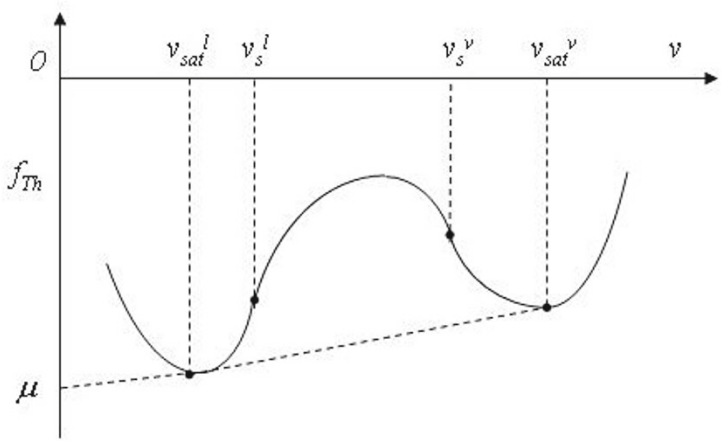

FIGURE 2. Typical double-well curve of the free energy of a single component fluid.

When $T_r < 1$ a typical curve of the free energy is represented in Figure 2. Now, keeping T_r fixed and considering that the two phases at equilibrium have the same

pressure, using the relation $P = -(\partial f_{Th}/\partial v)_T$, we obtain:

$$P^\alpha = P^\beta \quad \Longrightarrow \quad \left(\frac{\partial f_{Th}}{\partial v}\right)_T^\alpha = \left(\frac{\partial f_{Th}}{\partial v}\right)_T^\beta, \tag{2.20}$$

which, in Figure 2, represents the fact that the two equilibrium points have the same tangent. From this relation we can determine the specific volumes of the two phases at equilibrium, v_e^α and v_e^β. This relation can also be obtained considering that the specific volumes of the two phases at equilibrium minimize the total free energy, i.e.,

$$F_{Th} = \int \rho f_{Th}(\rho)\, d^3\mathbf{x} = \text{min.}, \tag{2.21}$$

where ρf_{Th} is the free energy per unit volume,

$$\rho f_{Th}(\rho) = \frac{kT}{m}[\rho \ln \rho + \rho^2 B(T)]. \tag{2.22}$$

This minimization is carried out in Section 3.1. In Figure 1, besides the equilibrium curve, we have represented the, so called, spinodal curve, defined as the locus of all points (like c and d) satisfying $(\partial P/\partial v)_T = 0$. When the equilibrium and spinodal points are plotted in a $T - v$ diagram, we obtain the curves of Figure 3. All points lying outside the region encompassing the equilibrium curve are stable and represent homogeneous, single-phase systems; all points lying inside the region within the bell-shaped spinodal curve are unstable and represent systems that will separate into two phases (one liquid and another vapor, in this case); the region sandwiched between the equilibrium and the spinodal curves represents metastable systems, that is overheated liquid and undercooled vapor. The spinodal points can be also determined using the relation $(\partial P/\partial v)_T = 0$, obtaining:

$$\left(\frac{\partial^2 f_{Th}}{\partial v^2}\right)_T = 0, \tag{2.23}$$

determining the spinodal specific volumes $\tilde{v}_s^\alpha$ and $\tilde{v}_s^\beta$.

3. The diffuse interface

3.1. The interfacial region

Suppose now that the density of the system is not constant. Accordingly, when $U_0 \ll kT$, Eq. (2.1) can be rewritten as

$$f(\mathbf{x}) = f_{Th}(\mathbf{x}) + \Delta f_{NL}(\mathbf{x}), \tag{3.1}$$

where f_{Th} is the specific free energy (2.2) corresponding to a system with constant density, while

$$\Delta f_{NL}(\mathbf{x}) = \frac{1}{2m^2}\int_{r>d} U(r)[\rho(\mathbf{x}+\mathbf{r}) - \rho(\mathbf{x})]d^3\mathbf{r} \tag{3.2}$$

is a non-local specific free energy, due to density changes, typical of the diffuse interface model. In fact, when there is an interface separating two phases at equilibrium, this term corresponds to the interfacial energy. This result is a direct consequence

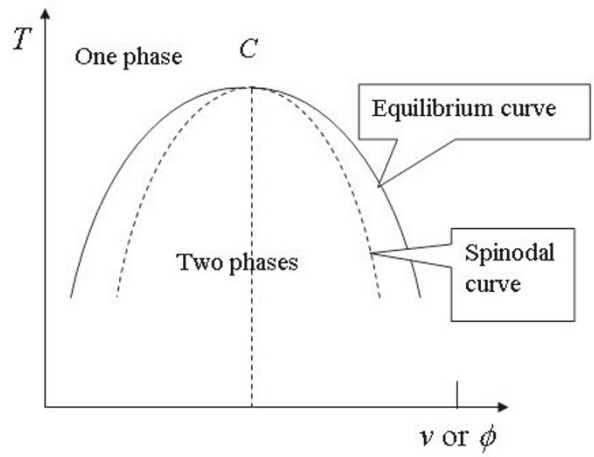

FIGURE 3. Phase diagram $(T - v)$ of a single component fluid and $(T - \phi)$ of a binary mixture.

of the "exact" expression (2.1), showing that the free energy is non-local, that is its value at any given point does not depend only on the density at that point, but it depends also on the density at neighboring points. As stated by van der Waals [59], "the error that we commit in assuming a dependence on the density only at the point considered vanishes completely when the state of equilibrium is that of a homogeneous distribution of the substance. If, however, the state of equilibrium is one where there is a change of density throughout the vessel, as in a substance under the action of gravity, then the error becomes general, however feeble it may be." Now, in (3.2) the density can be expanded as

$$\rho(\mathbf{x}+\mathbf{r}) = \rho(\mathbf{x}) + \mathbf{r}\cdot\nabla\rho + \frac{1}{2}\mathbf{rr} : \nabla\nabla\rho + \dots \tag{3.3}$$

As we have tacitly assumed that the system is isotropic, we see that the contribution of the linear term vanishes, so that, at leading order, we obtain [43]:

$$\Delta f_{NL}(\mathbf{x}) = -\frac{1}{2}K\nabla^2\rho(\mathbf{x}), \tag{3.4}$$

with

$$K = \frac{2\pi}{3}\frac{U_0\ell^6}{m^2 d} = \frac{9\pi}{4}\frac{kT_C d^5}{m^2}, \tag{3.5}$$

where we have substituted Eqs. (2.3), (2.8) and (2.15). Note that, defining a non-dimensional density, $\tilde{\rho} = d^3\rho/m$, the non-local free energy can be rewritten as

$$\Delta f_{NL}(\mathbf{x}) = -\frac{1}{2}\frac{kT}{m}a^2\nabla^2\tilde{\rho}(\mathbf{x}), \tag{3.6}$$

where

$$a = \sqrt{\frac{Km^2}{kTd^3}} = \sqrt{\frac{9\pi T_C}{4T}}d \tag{3.7}$$

is the characteristic length.

Comment. In the previous analysis, we have truncated the expansion (3.3) after the second-order term, neglecting the next significant (i.e. the fourth-order) term. That means assuming that $\epsilon = a^2/\lambda^2 \ll 1$, where λ denotes the thickness of the interfacial region. Now, although this assumption is satisfied near the critical point, where λ diverges as $T \to T_C$ [cf. Eq. (3.25)], far from the critical point, ϵ is not too small. Consequently, one might conclude that a fully non-local theory should be employed, which, however, leads to quite complicated governing equations, as shown by Rohde [50]. Fortunately, comparing local and non-local approaches, Frezzotti *et al.* [13] showed that the mean field approximation seems to capture, even quantitatively, the main features of the process. The explanation of this result is that, at a water-vapor or an oil-water interface, $\epsilon \approx 0.1$, so that we expect the mean field approximation to be correct within a 10% error.

Now, the total free energy is the sum of the volume integral,

$$\int_V \rho f d^3\mathbf{x} = \int_V \rho \left(f_{Th} - \frac{1}{2} K \nabla^2 \rho \right) d^3\mathbf{x}, \tag{3.8}$$

where ρf is the free energy per unit volume, and a surface contribution. In fact, at the wall, the non-local free energy (3.2) becomes,

$$\frac{1}{2m^2} \oint \left\{ \rho_s(\mathbf{x}) \left[\int U(r)\, \rho(\mathbf{x}+\mathbf{r})\, d^3\mathbf{r} \right] \right\} d^2\mathbf{x} = \oint f_w(\rho(\mathbf{x}))\, d^2\mathbf{x}, \tag{3.9}$$

where the integration is carried out on the surface. Here, ρ_s is the surface density and f_w is the wall free energy per unit surface, that we assume to be a function of the fluid density at the wall only. Now, observing that, integrating by parts,

$$\int \rho(\mathbf{x}) \nabla^2 \rho(\mathbf{x}) d^3\mathbf{x} = \oint \mathbf{n} \cdot (\rho \nabla \rho)\, d^2\mathbf{x} - \int |\nabla \rho(\mathbf{x})|^2 d^3\mathbf{x}, \tag{3.10}$$

we see that the total free energy is the sum of a bulk and a surface free energy, i.e.,

$$F = F_b + F_w. \tag{3.11}$$

Here, F_w is the wall free energy,

$$F_w = \oint \left[-\frac{1}{2} K \mathbf{n} \cdot (\rho \nabla \rho) + f_w(\rho) \right] d^2\mathbf{x}, \tag{3.12}$$

while F_b is the bulk free energy,

$$F_b = \int \widehat{f}(\rho, \nabla\rho, T)\, d^3\mathbf{x}, \tag{3.13}$$

with

$$\widehat{f}(\rho, \nabla\rho, T) = \rho f_{Th}(\rho, T) + \frac{1}{2} K (\nabla\rho)^2 \tag{3.14}$$

denoting the bulk free energy per unit volume, with $f_{Th} = (kT/m)[\ln \rho + \rho B(T)]$.

Now we want to see how the non local term of the free energy will affect the chemical potential which, we remind, measures the free energy variation due to an isothermal volume change. We know that at equilibrium, keeping the temperature

T constant, the total free energy F will be minimized, subjected to the constraint of mass conservation, $\int \rho d^3\mathbf{x} = M$. Accordingly, introducing a Lagrange multiplier, $\rho\mu$, the minimization condition is:

$$\delta \int \left(\widehat{f} - \rho\mu \right) d^3\mathbf{x} + \delta \oint \left[-\frac{1}{2} K \mathbf{n} \cdot (\rho \nabla \rho) + f_w(\rho) \right] d^2\mathbf{x} = 0, \tag{3.15}$$

for any arbitrary variation $\delta\rho$ of the density field. Now, consider that, for any function $h(\rho, \nabla\rho)$, we have:

$$\delta h = \frac{\partial h}{\partial \rho}\delta\rho + \frac{\partial h}{\partial(\nabla_i \rho)}\delta(\nabla_i \rho), \quad \text{with } \delta(\nabla_i \rho) = \nabla_i(\delta\rho), \tag{3.16}$$

and

$$\int_V \frac{\partial h}{\partial \nabla_i \rho} \nabla_i(\delta\rho) d^3\mathbf{x} dt = \oint_S n_i \frac{\partial h}{\partial \nabla_i \rho} \delta\rho d^2\mathbf{x} - \int_V \nabla_i \left(\frac{\partial h}{\partial \nabla_i \rho} \right) \delta\rho d^3\mathbf{x}. \tag{3.17}$$

Applying these two equalities to Eq. (3.15) we obtain:

$$\int \left[\frac{\partial \widehat{f}}{\partial \rho} - \nabla_i \left(\frac{\partial \widehat{f}}{\partial \nabla_i \rho} \right) - \mu \right] \delta\rho d^3\mathbf{x} + \oint_S \mathbf{n} \cdot \left[\frac{1}{2} K \nabla\rho + \frac{df_w}{d\rho} \right] \delta\rho d^3\mathbf{x} = 0, \tag{3.18}$$

where we have considered that $\delta(\rho\nabla\rho) = \delta\rho\,\nabla\rho + \rho\nabla\delta\rho$ and assumed that $\mathbf{n}\cdot\nabla\delta\rho = 0$ at the boundary.

3.2. The generalized chemical potential

Choosing $\delta\rho = 0$ at the boundary, Eq. (3.18) reduces to minimizing the bulk free energy. So, predictably, we obtain the Euler-Lagrange equation:

$$\mu = \frac{\partial \widehat{f}}{\partial \rho} - \nabla_i \left(\frac{\partial \widehat{f}}{\partial \nabla_i \rho} \right), \tag{3.19}$$

that is,

$$\mu = \frac{\delta(\rho f)}{\delta \rho} = \frac{d(\rho f_{Th})}{d\rho} - K\nabla^2\rho. \tag{3.20}$$

Now, by definition, the first term on the RHS is the Gibbs free energy, which, in a one-component system, coincides with the chemical potential, since,

$$\mu_{Th} = \frac{d(\rho f_{Th})}{d\rho} = f_{Th} + Pv, \tag{3.21}$$

where $P = -df_{Th}/dv$ (this is the slope of the tangent line represented in Figure 2). Therefore, Eq. (3.19) can be rewritten as

$$\mu(\rho, \nabla\rho) = \mu_{Th}(\rho) - K\nabla^2\rho, \tag{3.22}$$

showing that at equilibrium, when ρ is non-uniform, it is μ, and not μ_{Th}, that remains uniform. Note that the thermodynamic chemical potential, μ_{Th}, can be determined from the solvability condition of Eq. (3.21), that is,

$$\mu_{Th} = \frac{\rho^\alpha f^\alpha_{Th} - \rho^\beta f^\beta_{Th}}{\rho^\alpha - \rho^\beta} = \frac{v^\alpha f^\beta_{Th} - v^\beta f^\alpha_{Th}}{v^\alpha - v^\beta}, \tag{3.23}$$

as can also be seen geometrically from Figure 2, stating that the chemical potential equals the intercept of the tangent line on the $v = 0$ vertical axis. When two phases are coexisting at equilibrium, separated by a planar interfacial region centered on $z = 0$, Eq. (3.19) can be solved once the equilibrium free energy f is known, imposing that, far from the interface region, the density is constant and equal to its equilibrium value, so that the generalized chemical potential is equal to its thermodynamic value (3.21). In particular, in the vicinity of the critical point, considering that the chemical potential vanishes and expanding the free energy (2.19) as a power series of $\widetilde{v} = (v - v_C)/v_C$ and $\widetilde{t} = (T - T_C)/T_C$, with $v_C = 3c_2 = 2\pi d^3/m$, we obtain at leading order the following equation:

$$\frac{d^2\tilde{v}}{d\tilde{z}^2} - 6\tilde{t}\tilde{v} - \frac{3}{2}\tilde{v}^3 = 0, \tag{3.24}$$

where $\tilde{z} = z/\lambda$ is based on the characteristic length

$$\lambda = \sqrt{\frac{1}{8(-\tilde{t})}}d. \tag{3.25}$$

Equation (3.24) must be solved imposing that

$$\tilde{v}(\tilde{z} \to \pm\infty) = \pm\tilde{v}_e = \pm 2\sqrt{-\tilde{t}}. \tag{3.26}$$

The solution, due to van der Waals, is:

$$\tilde{v}(\tilde{z}) = \tilde{v}_e \tanh \tilde{z}, \tag{3.27}$$

showing that λ is a typical interfacial thickness. As expected, the interfacial thickness diverges like $(-\tilde{t})^{-1/2}$ as we approach the critical point, while far from the critical point it is of $O(d)$. As shown in [36], this solution can be generalized to finite systems, obtaining a family of Jacobi's elliptic functions. Recently, [43] pointed out that Eq. (3.24) is flawed, as some of the neglected terms diverge at the critical point. In fact, Pismen showed that in the correct solution the specific volume tends to its equilibrium value as $|\tilde{z}|^{-3}$, instead of exponentially, as in the van der Waals solution.

3.3. The surface tension

In Section 3.1 we have seen that the total free energy is the sum of a thermodynamical, constant density, part, and a non local contribution (3.4). When the system is composed of two phases at equilibrium, separated by a plane interfacial region, we may define the surface tension as the excess free energy per unit area stored in this region. This quantity can be calculated by integrating the specific (i.e. per unit volume) free energy from (3.4) along a coordinate z perpendicular to the interface:

$$\sigma = \frac{1}{2}K\int_{-\infty}^{\infty}\left(\frac{d\rho}{dz}\right)^2 dz, \tag{3.28}$$

where we have considered that the thermodynamic free energy density is the same for the two phases and that, outside the interfacial region, the non-local free energy

is identically zero as density is constant. We see that, near the critical point,

$$\sigma \approx K\frac{(\Delta\rho_e)^2}{\lambda} \approx \frac{kT_C}{d^2}(-\tilde{t})^{3/2}, \tag{3.29}$$

where we have considered the specific volumes of the two phases at equilibrium, Eq. (3.26), in addition to Eqs. (3.5) and (3.25). In fact, using the density profile (3.27), Eq. (3.28) yields, for a van der Waals system:

$$\sigma = C\frac{kT_C}{d^2}(-\tilde{t})^{3/2}, \tag{3.30}$$

with $C = 3^{3/2}/(2^{3/2}\pi)$, where we have used Eq. (2.16). These results show that the surface tension decreases as we approach criticality, until it vanishes at the critical point. A more detailed numerical solution based on the solution of the van der Waals equation can be found in [44]. Applying this approach, [59] showed that in a curved interface region there arises a net force which is compensated by a pressure term, thus obtaining the Young-Laplace equation. To see that, let us denote the position of the interface by $z = h(\xi)$, where ξ is the 2D vector in the tangent plane, and assume that $|\nabla_\xi h| \ll 1$, where $|\nabla_\xi h|$ is the 2D gradient [43]. Now, the free energy increment due to the interface curvature can be written as:

$$\Delta F = \sigma \int \left(\sqrt{1+|\nabla_\xi h|^2} - 1\right) d^2\xi \approx \frac{1}{2}\sigma \int |\nabla_\xi h|^2 d^2\xi. \tag{3.31}$$

This increment in the free energy induces an increment in the pressure,

$$\Delta P = \delta\Delta F/\delta h = -\sigma\nabla^2 h = -\kappa\sigma, \tag{3.32}$$

where $\kappa = \nabla^2 h$ is the curvature of a weakly curved interface. Applying a rigorous regular perturbation approach to Eq. (3.19), Pismen & Pomeau [44] derived both the Young-Laplace equation (3.32) and the Gibbs-Thomson law, relating the equilibrium temperature or pressure to the interfacial curvature.

3.4. The boundary conditions

As previously noted, the equilibrium state of an unconfined van der Waals fluid can be determined using the generalized chemical potential in the bulk. In general, however, for confined systems surface wettability effects are present and must be taken into account. In our D.I. approach such effects can be accounted for by introducing the simplest additional surface contribution to the free energy functional, which is based on the assumption that wettability is a local quantity, depending on the density of the two-phase fluid at the wall. Accordingly, choosing $\delta\rho = 0$ in the bulk, Eq. (3.18) reduces to minimizing the surface integral, and so we obtain the following boundary condition [22]:

$$\frac{1}{2}K\mathbf{n}\cdot\nabla\rho = -\frac{df_w}{d\rho}(\rho), \tag{3.33}$$

(with f_w denoting the wall surface energy) expressing a diffusively controlled local equilibrium at the wall. Now, assume the following linear dependence,

$$f_w(\phi) = \sigma_{\beta,w} + (\sigma_{\alpha,w} - \sigma_{\beta,w})\phi, \tag{3.34}$$

with $\phi = (\rho - \rho_\beta)/(\rho_\alpha - \rho_\beta)$ indicating the mass fraction of phase α while ρ_α and ρ_β denote the densities of the phases α and β at equilibrium. Therefore, and considering that $\sigma \cong a\rho kT/m$ is the surface tension between the two fluid phases at equilibrium, Eq. (3.33) can be rewritten as

$$\sigma\, a\, \mathbf{n} \cdot \nabla\phi = -\Delta\sigma_w, \tag{3.35}$$

where $\Delta\sigma_w = \sigma_{\alpha,w} - \sigma_{\beta,w}$ expresses the affinity of the wall to phase β, as compared to phase α. This condition is generally referred to as the Cahn boundary condition [4]. In the sharp interface limit, $\mathbf{n} \cdot \nabla\phi = \cos\theta$, where θ is the contact angle, and therefore the Cahn boundary condition reduces to the Young-Laplace formula, $\cos\theta = -\Delta\sigma_w/\sigma$. From here we see that, when $\sigma_{\alpha,w} = \sigma_{\beta,w}$ or when $\sigma_{\alpha,w}$ and $\sigma_{\beta,w}$ are both $\ll \sigma$, then $\theta = \pi/2$; instead, when $\sigma_{\alpha,w} \gg \sigma_{\beta,w}$ or $\sigma_{\alpha,w} \ll \sigma_{\beta,w}$, then $\theta = \pi$ and $\theta = 0$, respectively.

4. Equations of motion

4.1. Hamilton's principle

In this Section, we confine ourselves to the study of reversible motions of a dissipation-free fluid, where the effects of spatial inhomogeneities in the fluid density are accounted for within the van der Waals mean field theory, neglecting all surface contributions. The governing equations are obtained from Hamilton's minimum action principle:

$$S = \int_0^t \int_V \mathfrak{L}(\mathbf{v}, \rho, \nabla\rho) d^3\mathbf{x} dt = min., \tag{4.1}$$

where

$$\mathfrak{L}(\mathbf{v}, \rho, \nabla\rho) = \frac{1}{2}\rho\mathbf{v}^2 - \rho u(\rho, \nabla\rho) \tag{4.2}$$

is the Lagrangian density of the system, with u denoting the internal energy per unit mass. The minimization must be carried out with the constraints of conservation of mass and entropy, i.e.,

$$\dot\rho \equiv \frac{d\rho}{dt} = -\rho\nabla\cdot\mathbf{v}, \qquad \dot s = 0, \tag{4.3}$$

where s is the specific entropy per unit mass, while

$$\frac{d}{dt} = \frac{\partial}{\partial t} + \mathbf{v}\cdot\nabla \tag{4.4}$$

is the material, or Lagrangian, derivative. Accordingly, the relevant first variation is:

$$\delta \int_0^t \int_V \left\{ \frac{1}{2}\rho\mathbf{v}^2 - \rho u + \alpha\left[\dot\rho + \rho\nabla\cdot\mathbf{v}\right] - \beta\rho\dot s - \rho\boldsymbol{\gamma}\cdot\dot{\mathbf{x}}_0 \right\} d^3\mathbf{x} dt = 0, \tag{4.5}$$

where the vector field $\mathbf{x}_0 = \mathbf{x}_0(\mathbf{x}, t)$ establishes the initial position of a fluid particle which occupies the position $\mathbf{x}$ at time t. This form of Hamilton's principle for the compressible Euler equation was first presented by [19]. That treatment, however, allowed only for irrotational flows since it neglected the additional constraint of conservation of the identity of fluid particles, $d\mathbf{x}_0/dt = 0$. However, as noted by

Serrin [54], this last constraint is necessary to describe the most general unsteady motion of a compressible fluid.

The internal energy per unit mass in Eq. (4.2), consistent with the expression (3.14) for the generalized Helmholtz free energy per unit volume in the bulk, can be written as $u = u_{Th} + \Delta u_{NL}$, where $u_{Th} = f_{Th} + Ts$ is the thermodynamic free energy per unit mass, while Δu_{NL} is the non-local component of the specific internal energy (and of the free energy as well, since there is no non-local component of the specific entropy), given by:

$$\Delta u_{NL} = \frac{1}{2}\frac{K}{\rho}(\nabla\rho)^2. \tag{4.6}$$

The separate variations in ρ, $\mathbf{v}$, s and $\mathbf{x}_0$ (subject to the constraints above) which make the variational integral stationary lead to the following equations:

$$\delta\mathbf{v}: \quad \mathbf{v} = \nabla\alpha + \beta\nabla s + \boldsymbol{\gamma}\cdot\nabla\mathbf{x}_0, \tag{4.7}$$

$$\delta\rho: \quad \frac{d\alpha}{dt} = \frac{\mathbf{v}^2}{2} - \rho\left(\frac{\partial u_{Th}}{\partial\rho}\right)_s - u_{Th} + K\nabla^2\rho, \tag{4.8}$$

$$\delta s: \quad -\rho\left(\frac{\partial u_{Th}}{\partial s}\right)_\rho + \rho\frac{d\beta}{dt} = 0, \tag{4.9}$$

$$\delta\mathbf{x}_0: \quad \frac{d\boldsymbol{\gamma}}{dt} = 0. \tag{4.10}$$

These relations can be shown to imply the Euler equation for a compressible, inhomogeneous van der Waals fluid. In fact, from Eq. (4.7) one obtains the fluid acceleration as ([54])

$$\frac{d\mathbf{v}}{dt} = -\nabla\left(\frac{\mathbf{v}^2}{2}\right) + \nabla\frac{d\alpha}{dt} + \frac{d\beta}{dt}\nabla s, \tag{4.11}$$

which can be rearranged to the form,

$$\rho\frac{d\mathbf{v}}{dt} = -\nabla P + K\rho\nabla\nabla^2\rho, \tag{4.12}$$

where $P = \rho^2\left(\partial u_{Th}/\partial\rho\right)$ is the thermodynamic pressure. This derivation generalizes that by Serrin [54], taking into account the effect of the non-local component of the internal energy. As a result, in addition to the usual Euler equation, we obtain the last term on the RHS of Eq. (4.12), which is a reversible, so-called Korteweg, body force, driven by density gradients in the fluid. The same result can be obtained by applying Noether's theorem, as shown in [1].

As previously noted, Eq. (4.12) must be coupled to the continuity condition,

$$\frac{d\rho}{dt} + \rho\nabla\cdot\mathbf{v} = 0, \tag{4.13}$$

and the specific entropy equation, which, for non-dissipative systems, includes only the convective term, i.e.,

$$\rho\frac{ds}{dt} = \frac{\partial(\rho s)}{\partial t} + \nabla\cdot(\rho s\mathbf{v}) = 0. \tag{4.14}$$

4.2. The Korteweg stresses

The equation of motion can also be written as:

$$\rho\frac{d\mathbf{v}}{dt} = -\nabla P + \nabla\cdot\left\{K\left[\left(\rho\nabla^2\rho + \frac{1}{2}|\nabla\rho|^2\right)\mathbf{I} - \nabla\rho\otimes\nabla\rho\right]\right\}, \tag{4.15}$$

that is:

$$\rho\frac{dv_i}{dt} + \nabla_i\widetilde{p} = \nabla_j P^K_{ji}, \tag{4.16}$$

where, taking into account the expressions (3.19)-(3.21) for the chemical potential μ,

$$\widetilde{p} = P - K\left[\rho\nabla^2\rho + \frac{1}{2}(\nabla\rho)^2\right] = \mu\rho - \widehat{f} \tag{4.17}$$

is a pressure term (again $P = \rho^2 df_{Th}/d\rho$ is the thermodynamic pressure) and with P^K_{ij} denoting the Korteweg stress tensor [25]

$$P^K_{ij} = -K(\nabla_i\rho)(\nabla_j\rho) = -\frac{\partial\widehat{f}}{\partial(\nabla_i\rho)}\nabla_j\rho, \tag{4.18}$$

where we have used the expression (3.13) for the free energy per unit volume, i.e., $\widehat{f} = \rho f_{Th}(\rho) + \frac{1}{2}K(\nabla\rho)^2$. Note that the Korteweg stress and force depend only on the non-local part of the free energy, even when it is not explicitly indicated.

The divergence of the Korteweg stresses in Eq. (4.16) can also be rewritten as:

$$\nabla_j P^K_{ji} = -\left[\nabla_j\left(\frac{\partial\widehat{f}}{\partial\nabla_j\rho}\right)\nabla_i\rho + \frac{\partial\widehat{f}}{\partial\nabla_j\rho}\nabla_i\nabla_j\rho + \frac{\partial\widehat{f}}{\partial\rho}\nabla_i\rho - \frac{\partial\widehat{f}}{\partial\rho}\nabla_i\rho\right], \tag{4.19}$$

that is

$$\nabla\cdot\mathbf{P}^K = \mu\nabla\rho - \nabla\widehat{f}, \tag{4.20}$$

and therefore the momentum equation becomes

$$\rho\frac{d\mathbf{v}}{dt} + \nabla p' = \mu\nabla\rho, \tag{4.21}$$

where the pressure term has been redefined as

$$p' = \widetilde{p} + \widehat{f} = \rho\frac{d}{d\rho}(\rho f_{Th}) - K\rho\nabla^2\rho = \mu\rho. \tag{4.22}$$

Consequently, the momentum equation can be rearranged to the form:

$$\rho\frac{d\mathbf{v}}{dt} = -\rho\nabla\mu, \tag{4.23}$$

and, considering that $\rho\nabla\mu_{Th} = \nabla P$, we find again Eq. (4.12), i.e.,

$$\rho\frac{d\mathbf{v}}{dt} + \nabla P = \rho\mathbf{F}^K; \qquad \mathbf{F}^K = -\nabla\psi, \tag{4.24}$$

with

$$\psi = \mu_{NL} = -K\nabla^2\rho, \tag{4.25}$$

indicating that the non-local part of the generalized chemical potential, μ_{NL}, is a sort of potential energy; in fact, we can include into $\mathbf{F}^K$ also the contributions of any other potential force. For example, since the body force due to gravity is $\mathbf{F}_g = -\rho g\nabla z$,

where g is the gravity acceleration term and z is the vertical coordinate, this force can be accounted for by simply assuming in Eq. (4.24) that $\psi = \mu_{NL} + gz$.

It is interesting to observe that in near-equilibrium systems the Korteweg force is non-zero only in the narrow regions separating the different phases and therefore it is not surprising that it can also be expressed as the divergence of a tensor, just as it happens to surface forces.

Finally, we stress again that the Korteweg body force $\mathbf{F}^K$ is non dissipative, as it arises from the minimum action principle. Its expression in (4.24) is quite intuitive: being proportional to the gradient of the chemical potential (with a minus sign), it pushes the system towards thermodynamic equilibrium and is identically zero at equilibrium. In addition, since this force is reversible, it does not enter explicitly into the energy dissipation term.

4.3. Multicomponent systems and dissipative terms

In the case of a mixture composed of n species, defining the mass fraction of species k, $\phi^{(k)} = \rho^{(k)}/\rho$, as the ratio between the density (mass per unit volume) of species k and the total density, we have:

$$\sum_{k=1}^{n} \rho^{(k)} = \rho, \qquad \sum_{k=1}^{n} \phi^{(k)} = 1. \tag{4.26}$$

Now, the Korteweg force $\mathbf{F}^K$ for a mixture becomes:

$$\mathbf{F}^K = -\sum_{k=1}^{n} \phi^{(k)} \nabla \psi^{(k)}, \qquad \psi^{(k)} = \mu_{NL}^{(k)} + gz, \tag{4.27}$$

where $\psi^{(k)}$ is the sum of the non-local chemical potential of component k, $\mu_{NL}^{(k)}$, and of the potential of any other conservative external force, such as gravity. Therefore, since the Korteweg body force (4.27) has the general form of a potential force, we can apply all the results of irreversible thermodynamics (see de Groot and Mazur [10]). In particular, the rate of change of the mass of component k can be determined applying a general conservation equation, in terms of the mass flux of component k, $\mathbf{J}^{(k)} = \rho^{(k)}\mathbf{v}^{(k)}$, with $\mathbf{v}^{(k)}$ denoting the velocity of species k, obtaining:

$$\frac{\partial \left(\rho\phi^{(k)}\right)}{\partial t} + \nabla \cdot \left(\rho\phi^{(k)}\mathbf{v}^{(k)}\right) = 0, \qquad (k = 1, 2, \ldots, n) \tag{4.28}$$

where we have omitted the source term, indicating that the total mass of each species is conserved, therefore assuming that no chemical reaction takes place within the mixture. Generalization to reactive mixtures is straightforward [10]. Summing Eq. (4.28) over all k's we obtain the continuity equation, Eq. (4.13), with $\mathbf{v}$ indicating the mass-averaged, or barycentric, velocity,

$$\mathbf{v} = \frac{1}{\rho}\sum_{k=1}^{n} \rho^{(k)}\mathbf{v}^{(k)} = \sum_{k=1}^{n} \phi^{(k)}\mathbf{v}^{(k)}. \tag{4.29}$$

In particular, d/dt denotes the material derivative (4.4), expressed in terms of the barycentric velocity.

The balance equation of chemical species k can also be written as follows:

$$\rho\frac{d\phi^{(k)}}{dt} = -\nabla\cdot\mathbf{J}^{(k)}, \qquad (k=1,2,\ldots,n) \tag{4.30}$$

where the diffusive mass flux

$$\mathbf{J}^{(k)} = \rho\phi^{(k)}\left(\mathbf{v}^{(k)}-\mathbf{v}\right) \tag{4.31}$$

is defined in terms of the relative velocity of species k with respect to the barycentric velocity.

In the same way, conservation of momentum and energy lead to the following equations (see Eq. (19), (20) and (34) of Ch. II in [10]):

$$\rho\frac{d\mathbf{v}}{dt} + \nabla\cdot\mathbf{J}_{\mathbf{v}} = \rho\mathbf{F}^K, \tag{4.32}$$

and

$$\rho\frac{du}{dt} + \nabla\cdot\mathbf{J}_q = \dot{q}, \tag{4.33}$$

where $\mathbf{J}_{\mathbf{v}}$ and $\mathbf{J}_q$ are diffusive momentum and heat fluxes, respectively, while $\dot{q}$ is the heat source, given by

$$\dot{q} = -\mathbf{J}_{\mathbf{v}}:\nabla\mathbf{v} - \sum_{k=1}^{n}\mathbf{J}^{(k)}\cdot\nabla\mu_{NL}^{(k)}, \tag{4.34}$$

showing that the heat source, i.e the conversion of mechanical energy into heat, is due to momentum and mass diffusion. The diffusive fluxes $\mathbf{J}^{(k)}$, $\mathbf{J}_{\mathbf{v}}$ and $\mathbf{J}_q$ are determined through appropriate constitutive relations. To understand the form of these equations, we consider the entropy production term (see Eq. (13) of Ch. IV in [10]),

$$\sigma^{(S)} = -\frac{1}{T}\mathbf{J}_s\cdot\nabla T - \sum_{k=1}^{n-1}\frac{1}{T}\mathbf{J}^{(k)}\cdot\left[\nabla\mu^{(kn)}\right]_T - \frac{1}{T}\widetilde{\mathbf{J}}_{\mathbf{v}}:\nabla\mathbf{v}, \tag{4.35}$$

with $\mu^{(kn)} = \mu^{(k)} - \mu^{(n)}$, where the subscript T indicates that the gradient is taken at constant temperature, and we have considered that μ_{NL} is not an explicit function of T. Here, $\mathbf{J}_s$ is the entropy flux,

$$\mathbf{J}_s = \frac{1}{T}\left(\mathbf{J}_q - \sum_{k=1}^{n}\mathbf{J}^{(k)}h_{Th}^{(k)}\right), \tag{4.36}$$

where $h_{Th}^{(k)}$ is the thermodynamic partial enthalpy of species k, while

$$\widetilde{\mathbf{J}}_{\mathbf{v}} = \mathbf{J}_{\mathbf{v}} - P\mathbf{I} \tag{4.37}$$

is a corrected momentum flux, in which the thermodynamic pressure term has been subtracted. Note that, since $\mu = \mu_{Th} + \mu_{NL}$, the diffusive flux in (4.35) is associated with two forces, one being the diffusion driving force, $\nabla\mu_{Th}$, the other being the non-local, out-of-equilibrium Korteweg force, $\nabla\mu_{NL}$ which, as we saw, plays the role of a potential external force. Then, applying the Onsager reciprocity relations, neglecting all coupling terms (i.e. thermo-diffusion and Dufour effects), we see that, for regular,

isotropic fluids, the heat flux, $\mathbf{J}_q$, the momentum tensor, $\mathbf{J}_\mathbf{v}$, and the chemical species diffusive flux, $\mathbf{J}^{(i)}$, can be expressed through the following constitutive equations:

$$\mathbf{J}_q = -k\nabla T + \sum_{k=1}^{n} \mathbf{J}^{(k)} h_{Th}^{(k)}, \tag{4.38}$$

$$\mathbf{J}_\mathbf{v} = \left[P - \lambda\left(\nabla\cdot\mathbf{v}\right)\right]\mathbf{I} - \eta\left(\nabla\mathbf{v} + \nabla\mathbf{v}^{+}\right), \tag{4.39}$$

and

$$\mathbf{J}^{(i)} = -\rho \sum_{i\neq k=1}^{n-1} L^{(ik)} \left[\nabla\mu^{(kn)}\right]_T, \tag{4.40}$$

where k and η denote thermal conductivity and shear viscosity, respectively, $\lambda = \zeta - 2\eta/3$, with ζ indicating the bulk viscosity while $L^{(ik)}$ denotes the diffusivity of i into k; all these coefficients are local functions of temperature, pressure and composition. Finally, note that, although the last term in (4.36) can be either positive or negative, substituting the constitutive relation (4.38) into (4.36), we see that the first term on the RHS of (4.35) is always positive, as it must be; the same happens also when the coupling terms are taken into account.

The heat generation term and the internal energy flux in Eq. (4.33) can also be written in the following form:

$$\dot{q} = -\mathbf{J}_\mathbf{v} : \nabla\mathbf{v} - \rho\sum_{k=1}^{n} \mu_{NL}^{(k)} \frac{d\phi^{(k)}}{dt}, \tag{4.41}$$

and

$$\mathbf{J}_q = -k\nabla T + \sum_{k=1}^{n} \mathbf{J}^{(k)} h^{(k)}, \tag{4.42}$$

where $h^{(k)} = h_{Th}^{(k)} + \mu_{NL}^{(k)}$ denotes the total partial enthalpy of species k, i.e. its thermodynamic part plus its non local contribution.

5. Incompressible binary mixtures

Consider an incompressible binary mixture, where the continuity equation (4.13) reduces to

$$\nabla\cdot\mathbf{v} = 0. \tag{5.1}$$

Accordingly, the pressure appearing in the momentum equation has no real physical meaning, while the stress tensor reduces to

$$\mathbf{J}_\mathbf{v} = P\mathbf{I} - \eta\left(\nabla\mathbf{v} + \nabla\mathbf{v}^{+}\right), \tag{5.2}$$

and the Korteweg force becomes:

$$\mathbf{F}^K = -\phi\nabla\mu_{NL}, \tag{5.3}$$

where $\phi = \phi^{(1)}$ is the mass fraction of component 1, while $\mu_{NL} = \mu_{NL}^{(1)} - \mu_{NL}^{(2)}$ is the generalized non-local chemical potential difference.[1]

In the internal energy equation (4.33) the heat generation term (4.41) becomes

$$\dot{q} = -\mathbf{J}_{\mathbf{v}} : \nabla \mathbf{v} - \rho \mu_{NL} \frac{d\phi}{dt}, \tag{5.4}$$

while the internal energy flux (4.42) is expressed through the constitutive relation

$$\mathbf{J}_q = -k \nabla T + \mathbf{J}_\phi h. \tag{5.5}$$

Here, $\mu = \mu^{(1)} - \mu^{(2)}$ and $h = h^{(1)} - h^{(2)}$ are the total chemical potential and partial enthalpy difference, respectively, while $\mathbf{J}_\phi = \mathbf{J}^{(1)}$ is the diffusive flux of species 1, where we have considered that $\mathbf{J}^{(2)} = -\mathbf{J}^{(1)}$. In turn, the diffusive flux is expressed through the constitutive relation (4.40):

$$\mathbf{J}_\phi = -\rho L^* \left[\nabla \mu\right]_T, \tag{5.6}$$

where L^* is an effective diffusivity term. We remind here that, as in the single component case, the generalized chemical potential is the sum of the thermodynamic chemical potential plus any other potential. In our case, that means adding the effect of the non-local part of the free energy.

5.1. Regular incompressible binary mixtures

In the following, we will confine ourselves to the simplest case, when the two species composing the binary mixture have the same mass density, ρ and the same molecular weight, $M_w = N_A m$, so that mass, molar and volume fractions coincide with each other. Removing this assumption, although conceptually simple, involves introducing several additional terms in the governing equations (see [10], Ch. X1, §2), nevertheless without adding anything substantial to the model. This perfectly symmetric binary mixture can be considered as a very particular case of regular binary solutions, that are mixtures such that, when we mix the two species at constant temperature and pressure, a) the entropy change is equal to that of an ideal mixture, and b) the volume remains unchanged (see [52], Ch. 7.6). Defining an excess quantity as the difference between its value and that of an ideal gas, that means that both the excess volume of mixing and the excess entropy of mixing are equal to zero, i.e., $v_{ex} = 0$ and $s_{ex} = 0$.

The specific Gibbs free energy can be determined using the same procedure as for single component systems. Consider a mixture composed of species 1 and species 2, with mass (and also molar and volume) fraction $x^{(1)} = \phi$ and $x^{(2)} = 1 - \phi$ and let us first determine the specific free energy when the composition of the mixture is uniform. Considering the definition of Gibbs free energy, $g = f + P/\rho$, starting from Eq. (2.1) we obtain

$$g_{Th}(\phi) = g_{id}(\phi) + g_{ex}(\phi). \tag{5.7}$$

[1]The extra term that is obtained, $\nabla \mu_{NL}^{(2)}$, being the gradient of a scalar, can be absorbed into the pressure term.

Here, g_{id} is the Gibbs free energy of an ideal mixture, that is a mixture where the intermolecular potentials $U^{(ij)}$ between molecule i and molecule j are all the same, i.e. $U^{(11)} = U^{(22)} = U^{(12)}$. Generalizing the expression of the free energy for a single component fluid, $\frac{kT}{m} \ln \rho$, we obtain:

$$g_{id} = \frac{kT}{m} \left[x_1 \ln(x_1 \rho) + x_2 \ln(x_2 \rho) \right],$$

that is

$$g_{id} = \frac{kT}{m} \ln \rho + RT[\phi \log \phi + (1 - \phi) \log(1 - \phi)]. \tag{5.8}$$

Note that for a pure fluid the density ρ is a variable, while for a regular binary mixture the total density ρ can even be constant, since the variables are the molar densities of the two components, $x_1\rho$ and $x_2\rho$.

The second term in the RHS of Eq. (5.7), g_{ex}, is the so called excess, that is non ideal, part of the free energy, and can be determined starting from the fundamental expression (2.1) for the Helmholtz free energy and considering that:

$$g_{ex} = f_{ex} + P v_{ex}. \tag{5.9}$$

Applying Eqs. (2.5), (2.6) and (5.9) to a system with constant density ρ, i.e. with $v_{ex} = 0$, we obtain $g_{ex} = f_{ex} = \frac{kT}{m} \rho B$, where B is the virial coefficient:

$$B = x_1^2 B^{(11)} + 2 x_1 x_2 B^{(12)} + x_2^2 B^{(22)}. \tag{5.10}$$

Here, $B^{(ij)}$ characterizes the repulsive interaction between molecule i and molecule j [see Eq. (2.6)],

$$B^{(ij)} = \frac{1}{2m} \int \left[1 - \exp\left(-\frac{U^{(ij)}(r)}{kT} \right) \right] d^3\mathbf{r}, \tag{5.11}$$

where $U^{(ij)}$ is the pairwise interaction potential between molecules i and j. In particular, for symmetric solutions, $U^{(11)} = U^{(22)} \neq U^{(12)}$, so that $B^{(11)} = B^{(22)} \neq B^{(12)}$. Accordingly, denoting $x_1 = \phi$, we obtain:

$$g_{ex} = \frac{kT}{m} \rho B = 2\rho \frac{kT}{m} (B^{(12)} - B^{(11)}) \phi (1 - \phi),$$

that is

$$g_{ex}(T, P, \phi) = \frac{kT}{m} \Psi(T, P) \phi (1 - \phi), \tag{5.12}$$

where

$$\Psi(T, P) = 2\rho (B^{(12)} - B^{(11)}) \tag{5.13}$$

is the so called Margules coefficient [52]. In particular, for an ideal mixture, $B^{(11)} = B^{(12)}$ and therefore $\Psi = 0$. For a mixture composed of van der Waals fluids at constant pressure, substituting the expression (2.7) for B and assuming that the characteristic lengths d and ℓ are the same for the two species, we obtain:

$$\Psi = \frac{2m\rho}{kT} (c_1^{(11)} - c_1^{(12)}) = \frac{4\pi}{3} \frac{\rho \ell^6}{kT m d^3} (U_0^{(11)} - U_0^{(12)}), \tag{5.14}$$

where $U_0^{(11)}$ and $U_0^{(12)}$ characterize the strength of the potential between molecules of the same species and that of different species, respectively. From this expression we see that $\Psi \propto T^{-1}$, confirming that g_{ex} is independent of T. Note that when $\Psi > 0$ the repulsive forces $\cong U_0^{(12)}/d$ between unlike molecules are weaker than those between like molecules, $\cong U_0^{(11)}/d$. As shown in [36], when the solution is not symmetric, this approach is easily generalized by defining two Margules coefficients.

5.2. Coexistence and spinodal curve

The thermodynamic state of a one-component system is determined by fixing two quantities, e.g. P and T. In incompressible binary mixtures, while pressure is irrelevant, we have an additional degree of freedom, i.e. the mass (or molar) fraction of one of the two species, $x^{(1)}$. Now, associated with $x^{(1)}$ and $x^{(2)}$ we can define the respective chemical potentials, $\mu_{Th}^{(1)} = \partial(Mg_{Th}/\partial M^{(1)})_{M^{(2)}}$ and $\mu_{Th}^{(2)} = \partial(Mg_{Th}/\partial M^{(2)})_{M^{(1)}}$, where $M^{(i)}$ is the mass of species i and $M = M^{(1)} + M^{(2)}$ is the total mass. Considering that $x^{(1)} = 1 - x^{(2)}$, there is a relation between $\mu^{(1)}$ and $\mu^{(2)}$, namely the Gibbs-Duhem relation [52], $x^{(1)}\nabla\mu_{Th}^{(1)} = -x^{(2)}\nabla\mu_{Th}^{(2)}$. This relation can be easily obtained considering the definition of the specific Gibbs free energy, g_{th},

$$g_{Th} = u_{Th} - Ts + Pv + x^{(1)}\mu_{Th}^{(1)} + x^{(2)}\mu_{Th}^{(2)}, \tag{5.15}$$

where u_{Th} is the specific (i.e. per unit mass) internal energy, and imposing that the following equality is satisfied,

$$dg_{Th} = -sdT + vdP + \mu_{Th}d\phi, \tag{5.16}$$

where $\mu_{Th} = \mu_{Th}^{(1)} - \mu_{Th}^{(2)}$ is the thermodynamic chemical potential difference. Note that this last relation reveals that the chemical potential difference is the quantity which is thermodynamically conjugated with the composition ϕ. This same result can be obtained from the identities [52],

$$\mu_{Th}^{(1)}(T,\phi) = g_{Th}(T,\phi) + \left(\frac{dg_{Th}}{d\phi}\right)(1-\phi), \tag{5.17}$$

$$\mu_{Th}^{(2)}(T,\phi) = g_{Th}(T,\phi) - \left(\frac{dg_{Th}}{d\phi}\right)\phi. \tag{5.18}$$

In the previous Section, we saw that the free energy of a homogenous, regular, symmetric binary mixture can be written as:

$$g_{Th} = g_1 + \frac{kT}{m}\left[\phi\log\phi + (1-\phi)\log(1-\phi) + \Psi\phi(1-\phi)\right]. \tag{5.19}$$

Therefore, we obtain:

$$\mu_{Th} = \mu_{Th}^{(1)} - \mu_{Th}^{(2)} = \frac{d(g_{Th})}{d\phi} = \frac{kT}{m}\left[\log\left(\frac{\phi}{1-\phi}\right) + \Psi(1-2\phi)\right], \tag{5.20}$$

At constant temperature T (remind that the thermodynamic pressure P is irrelevant in incompressible fluids), since Ψ is a known function of T, this equation gives the dependence of the chemical potential difference on the composition, just like the equation of state, e.g. van der Waals' equation, gives the dependence of the pressure

on the specific volume. Clearly, μ_{Th} represents the tangent to the free energy curve and it is the same for the two phases at equilibrium. Accordingly, this equation leads to the determination of the equilibrium composition of the two coexisting phases, ϕ_e^α and ϕ_e^β. In particular, in our case, where we have considered symmetric mixtures, the tangent is horizontal and therefore $\mu_{Th} = 0$. Note that, as expected, in this case $\phi_e^\alpha = 1 - \phi_e^\beta$. Now we can apply to binary mixtures the same considerations about the critical point that we made in the previous Section on one-component systems, simply replacing pressure and density (or specific volume) with chemical potential difference μ_{Th} and composition ϕ, respectively. In particular, just like the $P - T$ single component phase diagram, the $\mu_{Th} - T$ liquid-liquid phase diagram stops at the critical point, characterized by a critical temperature T_C and a critical chemical potential difference, $\mu_C = 0$ (note that for symmetric mixtures $\mu_{Th} = 0$ at any equilibrium state, while in general that is true only at the critical point). At higher temperatures, $T > T_C$, the differences between the two liquid phases vanish altogether and the system is always in a single phase. In addition, as the critical point is approached from below (i.e. with two coexisting phases), the difference between the composition of the two phases decreases, until it vanishes altogether at the critical point, where, as in Eq. (2.12), we have:

$$\left(\frac{\partial \mu_{Th}}{\partial \phi}\right)_{T_C,P_C} = 0, \qquad \left(\frac{\partial^2 \mu_{Th}}{\partial \phi^2}\right)_{T_C,P_C} = 0. \tag{5.21}$$

This indicates that the critical point corresponds to a horizontal inflection point in the $\mu_{Th} - \phi$ diagram (see Figure 1). Therefore, from Eq. (5.20) we see that $\phi_C^\alpha = \phi_C^\beta = 1/2$, confirming that $\Psi_C = 2$. Therefore, considering that $\Psi \propto T^{-1}$, we obtain:

$$\Psi = \frac{2T_C}{T}. \tag{5.22}$$

Now, let us consider a liquid binary mixture at equilibrium, whose temperature is below its critical values, so that it is separated into two coexisting phases, α and β. As a reversible $\alpha - \beta$ phase transition takes place at constant temperature and chemical potential difference, it can be represented as a horizontal isotherm segment in a $\mu_{Th} - \phi$ diagram. Now, define a generalized potential [31, Ch. 85] as $\Phi_{Th} = g_{Th} - \mu_{Th}\phi$, with $d\Phi_{Th} = -sdT - \phi d\mu_{Th}$ and $(\partial \Phi_{Th}/\partial \mu_{Th})_T = -\phi$ (again, remind that pressure is irrelevant for incompressible mixtures). The chemical potential difference μ_{Th} at a given temperature and pressure can be easily determined, considering that at equilibrium the generalized potentials of the two phases must be equal to each other, that is,

$$\Phi_{Th}^\beta - \Phi_{Th}^\alpha = \int_b^e d\Phi_{Th} = 0 \quad \Longrightarrow \quad \int_b^e \phi \, d\mu_{Th} = [\mu_{Th}\phi]_b^e - \int_b^e \mu_{Th} d\phi = 0, \tag{5.23}$$

where we have considered that the phase transition is isothermal. From a geometrical point of view, this relation manifests the equality between the shaded area of Figure 1 (Maxwell's rule), where the points b and e correspond to the saturation points of the two phases at that temperature, with compositions ϕ^α and ϕ^β. Conversely, the

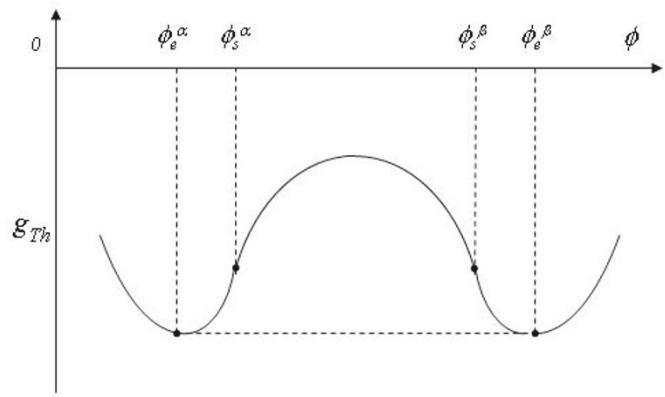

FIGURE 4. Typical double-well curve of the free energy of a symmetric binary mixture.

composition of the two coexisting phases at equilibrium can be determined considering that, at equilibrium, they have the same temperature and chemical potential (so that the chemical potential difference μ_{Th} is identically zero), obtaining:

$$\mu_{Th}^\alpha = \mu_{Th}^\beta = 0 \quad \Longrightarrow \quad \left(\frac{\partial g_{Th}}{\partial \phi}\right)_T^\alpha = \left(\frac{\partial g_{Th}}{\partial \phi}\right)_T^\beta \Longrightarrow \quad (\phi_e^\alpha, \phi_e^\beta), \tag{5.24}$$

which, in Figure 4, represents the fact that the two equilibrium points have the same tangent and this tangent is a horizontal line. When the mixture is not symmetric, the $g_{Th} - \phi$ curve is similar to the $f_{Th} - v$ curve of Figure 2. Consequently, in this case, it is still true that $\mu_{Th}^\alpha = \mu_{Th}^\beta$, but, in general, they are not equal to zero, i.e. the tangent to the Gibbs free energy curve is not horizontal. In Figure 1, besides the equilibrium curve, we have represented the, so called, spinodal curve, defined as the locus of all points (like c and d) satisfying $(\partial \mu_{Th}/\partial \phi)_T = 0$. When the equilibrium and spinodal points are plotted in a $T - \phi$ diagram, we obtain the curves of Figure 3. All points lying outside the region encompassing the equilibrium curve represent homogeneous, single-phase mixtures in a state of stable equilibrium, while all points lying inside that region represent systems in a state of non equilibrium, which tend to separate into two phases. However, all points lying in the region inside the spinodal curve are unstable, that is any infinitesimal perturbation can trigger the phase transition process, while all points sandwiched between the equilibrium and the spinodal curves represent metastable systems, i.e. mixtures that need an activation energy to phase separate. The spinodal points can be also determined using the relation $(\partial \mu_{Th}/\partial \phi)_T = (\partial^2 g_{Th}/\partial \phi^2)_T = 0$, obtaining:

$$\left(\frac{\partial^2 g_{Th}}{\partial \phi^2}\right)_T = 0 \quad \Longrightarrow \quad (\phi_s^\alpha, \phi_s^\beta). \tag{5.25}$$

5.3. The diffuse interface

Suppose now that the composition of the system is not constant. Proceeding as for single component systems, we have:

$$g(\mathbf{x}) = g_{Th}(\mathbf{x}) + \Delta g_{NL}(\mathbf{x}), \tag{5.26}$$

where Δg_{NL} is a non-local specific free energy (see Cahn & Hilliard [5]),

$$\Delta g_{NL} = \frac{kT}{2m} a^2 (\nabla \phi)^2. \tag{5.27}$$

Here, a is a characteristic length, roughly equal to the interface thickness at equilibrium which, for a regular mixture, has the same value as that seen in Eq. (3.7), i.e.,

$$a = \sqrt{\frac{9\pi T_C}{4T}} d, \tag{5.28}$$

where d is the excluded volume length defined in (2.8). Now, following the same procedure as in Section 3.3, observe that at the end of the phase segregation process, a surface tension σ can be measured at the interface and from that, as shown by [59], a can be determined as

$$a \approx \frac{\sigma M_w}{\rho RT}, \tag{5.29}$$

This relation can be easily derived considering that at equilibrium the surface tension σ is equal to the integral of the Cahn-Hilliard free energy across the interface, i.e. $\sigma \approx \rho \Delta g_{eq} a$, where $\Delta g_{eq} \approx kT/m$ is a typical value of the change in the Cahn-Hilliard specific free energy across the interface at equilibrium [59].

5.4. The generalized chemical potential

At equilibrium, the total free energy is minimized. As we saw in the previous Section, the minimization can be carried out separately in the bulk and at the boundaries. Accordingly, in the bulk we have:

$$\int_V g(\phi, \nabla\phi) d^3\mathbf{x} = min., \quad \text{with} \quad \int_V \phi(\mathbf{x}) d^3\mathbf{x} = const., \tag{5.30}$$

where the constraint of mass conservation has been applied. Therefore, applying to the system a virtual change in composition, $\delta\phi(\mathbf{x})$, we obtain the following Euler-Lagrange equation,

$$\mu = \frac{\delta g}{\delta \phi} = \frac{\partial g}{\partial \phi} - \nabla_i \frac{\partial g}{\partial(\nabla_i \phi)} = \mu_{Th}(\phi) - \nabla_i \frac{\partial g}{\partial(\nabla_i \phi)}, \tag{5.31}$$

where μ_{Th} is the thermodynamic chemical potential difference. This equation defines the generalized chemical potential difference, μ, and shows that μ, and not μ_{Th}, is uniform at equilibrium. Finally, substituting Eqs. (5.20), (5.26) and (5.27) into (5.31), we obtain:

$$\mu(\phi, \nabla\phi) = \mu_{Th}(\phi) - \frac{kT}{m} a^2 \nabla^2 \phi. \tag{5.32}$$

As for the boundary conditions, the same considerations of Section 3.4 can be applied to binary mixtures as well.

5.5. The diffusive mass flux

When the Cahn-Hilliard part of the free energy is neglected, the isothermal mass flux of component 1 is proportional to the gradient of the chemical potential of component 1 as (see Cussler [8], p. 180),

$$\mathbf{J}^{(1)} = -\rho D x^{(1)} \left[\nabla \widetilde{\mu}^{(1)}_{Th}\right]_T , \tag{5.33}$$

where $\widetilde{\mu}^{(1)}_{Th} = (m/kT)\,\mu^{(1)}_{Th}$ is a non-dimensional chemical potential, while D is the molecular diffusivity, which is a function of temperature and pressure, but not of composition. As we see below, the proportionality term $(Dx^{(1)})$ in (5.33) has been chosen so that in the ideal case we obtain Fick's constitutive law. For symmetric binary mixtures, substituting (5.19) into (5.17), we obtain the non-dimensional chemical potential as:

$$\widetilde{\mu}^{(1)}_{Th} = \widetilde{g}^{(1)} + \ln x^{(1)} + \Psi \left[x^{(2)}\right]^2 , \tag{5.34}$$

so that (5.33) yields:

$$\mathbf{J}^{(1)} = -\rho D x^{(1)} \left[\frac{d\widetilde{\mu}^{(1)}_{Th}}{dx^{(1)}} \nabla x^{(1)}\right]_T \quad \Longrightarrow \quad \mathbf{J}^{(1)} = -\rho D^* \left[\nabla x^{(1)}\right]_T , \tag{5.35}$$

where

$$D^* = D\left(1 - 2\Psi x^{(1)} x^{(2)}\right) \tag{5.36}$$

is the diffusion coefficient. Inverting the suffixes 1 and 2 in (5.35) and (5.36) we see that a) the diffusivity of component 1 into 2 equals the diffusivity of component 2 into 1, as it should, and b) the flux of species 2 is opposite to the flux of species 1, that is $\mathbf{J}^{(2)} = -\mathbf{J}^{(1)}$, showing that these are really diffusive fluxes, with no convective components.[2] From Eq. (5.36) we see that, for ideal or dilute mixtures, i.e. when either $\Psi = 0$, $x^{(1)} \ll 1$ or $x^{(2)} \ll 1$, we obtain that $D^* = D$ and therefore Eq. (5.35) reduces to Fick's law. In addition, when we plot D^* as a function of x_1 we see that for $\Psi > 2$ there is a region of negative diffusion, as it corresponds to the region of instability of the phase diagram. Going back to our notation, with $x_1 = \phi$, observe that, denoting $\mathbf{J}_\phi \equiv \mathbf{J}^{(1)}$ and considering that $\mathbf{J}^{(1)} + \mathbf{J}^{(2)} = 0$, the constitutive relation (5.33) can also be written as

$$\mathbf{J}_\phi = -\rho D \phi(1-\phi) \left[\nabla \widetilde{\mu}_{Th}\right]_T , \tag{5.37}$$

where $\mu_{Th} = \mu^{(1)}_{Th} - \mu^{(2)}_{Th}$, which coincides with (4.40), with $L^{(12)} = D\phi\,(1-\phi)$. Note that a Soret thermal diffusion term, accounting for the effect of temperature gradients, could also be added to the mass flux constitutive relation, although it is generally assumed to be negligible, as discussed in [58].

At this point, a natural extension of the constitutive relation (5.37) is to replace the thermodynamic chemical potential with the generalized chemical potential, thus

[2] In general, applying the Gibbs-Duhem relation to (5.33), we see that it is always true that $\mathbf{J}^{(2)} = -\mathbf{J}^{(1)}$ (see [42]).

obtaining Eq. (5.6) with $L^* = (Dm/kT)\phi(1-\phi)$, i.e.,

$$\mathbf{J}_\phi = -\rho D\phi(1-\phi)\left[\nabla\tilde{\mu}\right]_T. \tag{5.38}$$

This is the constitutive equation that has been used in [36] and in all subsequent works by Mauri and coworkers.

6. Summary of the equations of motion

6.1. The equations of motion for incompressible binary mixtures

In the case of incompressible regular binary mixtures, assuming that the fluid density ρ and the molecular weight M_w are constant, the conservation equation for chemical species, momentum and internal energy are [cf. Eqs. (4.30), (4.32) and (4.33)]:

$$\frac{d\phi}{dt} = -\nabla\cdot\mathbf{J}_\phi, \tag{6.1}$$

$$\rho\frac{d\mathbf{v}}{dt} = -\nabla\cdot\mathbf{J}_\mathbf{v} + \rho\mathbf{F}^K, \quad \nabla\cdot\mathbf{v} = 0, \tag{6.2}$$

$$\rho\frac{du}{dt} = -\nabla\cdot\mathbf{J}_q + \dot{q}, \tag{6.3}$$

where ϕ is the molar fraction of component 1, $\mathbf{J}_\phi$ is the diffusion flux, $\mathbf{v}$ the average local velocity of the fluid mixture (in our case, molar, mass and volume averages all coincide), $\mathbf{J}_\mathbf{v}$ the momentum flux tensor, $\mathbf{F}^K$ is the Korteweg force, including also any other external potential force, u the internal energy density, $\mathbf{J}_q$ and $\dot{q}$ the internal energy flux and the heat generation term, respectively.

In the conservation equation for the chemical species, the material diffusive flux, $\mathbf{J}_\phi$, must be coupled to the chemical potential gradient through the constitutive relation (5.38),

$$\mathbf{J}_\phi = -\phi(1-\phi)\,D\,\left[\nabla\tilde{\mu}\right]_T, \tag{6.4}$$

where D is the molecular diffusivity, the subscript "T" indicates constant temperature, and $\tilde{\mu}$ is the non-dimensional generalized chemical potential difference between the two species defined in (5.20), (5.31) and (5.32) as:

$$\widetilde{\mu} = \frac{\delta\widetilde{g}}{\delta\phi} = \log\left(\frac{\phi}{1-\phi}\right) + \Psi(1-2\phi) - a^2\nabla^2\phi, \tag{6.5}$$

where $\widetilde{g}$ is the non-dimensional free energy, including its non-local component [cf. Eq. (5.26)], a is a characteristic microscopic length and Ψ is the Margules parameter which describes the relative weight of enthalpic versus entropic forces. The single-phase region of the phase diagram corresponds to values $\Psi < 2$, with $\Psi = 2$ at the critical point, while, conversely, $\Psi > 2$ in the two-phase region. Accordingly, as Ψ is inversely proportional to the temperature, we conclude that

$$\Psi = \frac{2T_C}{T}. \tag{6.6}$$

The Navier-Stokes equation (6.2) must be supplemented by a constitutive equation for the stress tensor. For a Newtonian fluid, we have:

$$\mathbf{J_v} = P\mathbf{I} - \eta\left[\nabla\mathbf{v} + (\nabla\mathbf{v})^{+}\right], \tag{6.7}$$

with η denoting the composition-dependent fluid viscosity, while $\mathbf{I}$ is the identity dyadic and $(\nabla\mathbf{v})^{+}$ is the transpose of $\nabla\mathbf{v}$.

Finally, concerning the energy equation, the specific internal energy u is related to the temperature through the simple thermodynamic relation,

$$u = cT, \tag{6.8}$$

where c is the specific heat, assumed to be a known function of the composition ϕ. In addition, the heat generation term is [cf. Eq. (5.4)]

$$\dot{q} = -\mathbf{J_v} : \nabla\mathbf{v} - \frac{\rho RT}{M_w}\widetilde{\mu}_{NL}\frac{d\phi}{dt}, \tag{6.9}$$

where $\widetilde{\mu}_{NL} = -a^2\nabla^2\phi$ is the (non-dimensional) non-local part of the chemical potential difference, while the internal energy flux can be written as [cf. Eq. (5.5)]

$$\mathbf{J}_q = -k\nabla T + \frac{\rho RT}{M_w}\mathbf{J}_\phi\widetilde{h}, \tag{6.10}$$

where a Fourier constitutive relation for the heat flux has been assumed, with k denoting the mixture heat conductivity, which is a known function of the composition ϕ. Here, $\widetilde{h}$ is the total (thermodynamic plus non-local) non-dimensional partial enthalpy difference, which can be determined considering that $h = \mu + Ts$, obtaining:

$$\widetilde{h} = \Psi(1-2\phi) - a^2\nabla^2\phi. \tag{6.11}$$

The most important feature of this model is the presence in the governing equations (6.2) of the non-equilibrium reversible body force, $\mathbf{F}^K$, which equals the generalized gradient of the free energy and therefore it is driven by chemical potential gradients within the mixture,

$$\mathbf{F}^K = -\frac{RT}{M_w}\phi\nabla\tilde{\mu}_{NL}. \tag{6.12}$$

In particular, when the system presents well-defined phase interfaces, such as at the late stages of phase separation, this body force reduces to the more conventional surface tension, as shown by Jasnow & Viñals [23] and Jasmin [22]. Therefore, being proportional to gradients of the chemical potential difference, which are identically zero at local equilibrium, $\mathbf{F}^K$ can be thought of as a non-equilibrium capillary force. Since $\mathbf{F}^K$ is driven by surface energy, it tends to minimize the energy stored at the interface, resulting in a non-equilibrium attractive force between domains of the same phase, therefore driving, say, drops of the α phase towards regions of the same phase. Again, though, we should point out that in the presence of sharp interfaces the results of this continuous model should be taken *cum grano salis*.

Finally, note that if other potential forces are present within the system, $\mathbf{F}_{ext} = -\phi\nabla V_{ext}$, this potential can be simply added to $\tilde{\mu}_{NL}$ in Eq. (6.12).

In most of the our simulations concerning liquid binary mixtures, we have assumed that the viscosity of the mixture is a constant, independent of ϕ and that the Reynolds number is small. Accordingly, Eq. (6.2) reduces to the simpler Stokes equation:

$$\nabla P = \eta \nabla^2 \mathbf{v} + \rho \mathbf{F}^K, \qquad \nabla \cdot \mathbf{v} = 0. \tag{6.13}$$

The ratio between convective and diffusive mass fluxes defines the capillary Peclet number, $N_{Pe} = Va/D$, where V is a characteristic velocity, which can be estimated through (6.1) and (6.13), obtaining [61, 62]

$$N_{Pe} = \frac{Va}{D} \approx \frac{a^2}{D} \frac{\rho}{\eta} \frac{RT}{M_w} \approx \frac{\sigma a}{\eta D}. \tag{6.14}$$

Clearly, when N_{Pe} is small, the processes described by this model are always diffusion-driven. However, that happens only for systems with very large viscosities (e.g. polymer solutions), or in the vicinity of local equilibrium, when the body force $\mathbf{F}^K$ becomes negligibly small. Instead, low-viscosity liquid mixtures far from criticality and in condition of non-equilibrium (i.e. either phase-separating or mixing), are characterized by very large N_{Pe}, showing that convection dominates diffusion. Although this approach has been developed for very idealized systems, it seems to capture the main features of real mixtures.

6.2. The equations of motion for one-component fluids

Very similar results can be obtained for the equations of motion of one-component systems subjected to conservative forces. As we saw in Section 2, in this case the order parameter is the density ρ, which is different in the two phases. Therefore, the mixture is not incompressible, even when each phase can be assumed to be incompressible (think, for example, about a solid-liquid phase transition). Accordingly, the mass conservation equation is the usual continuity equation for compressible fluids. As van der Waals realized, the presence of the non-local term in the expression for the free energy has consequences in the determination of the remaining governing equations. As shown in [25], momentum conservation leads to a stress tensor where, in addition to the usual viscous stresses, there appears another, so-called Korteweg, stress,

$$\mathbf{P}^K = K \left[\nabla\rho \otimes \nabla\rho - \mathbf{I} \left(\rho \nabla^2 \rho + \frac{1}{2} |\nabla\rho|^2 \right) \right]. \tag{6.15}$$

Note that only the first term is anisotropic; the rest, in effect, contributes to a modification of the fluid pressure (which is obviously irrelevant in the incompressible binary mixture case seen before). When substituted into the momentum conservation balance, this term adds the so-called Korteweg force,

$$\mathbf{F}_K = -\nabla \cdot \mathbf{P}^K = -\rho \nabla \mu_{NL}, \tag{6.16}$$

to the usual Navier-Stokes equation for fluids of non-uniform density [cf. Eq. (4.24)]. Therefore, being proportional to the gradient of the chemical potential (with a minus sign), the Korteweg body force pushes the system towards thermodynamic equilibrium and is identically zero at equilibrium. In addition, since this force is reversible,

it does not enter explicitly into the energy dissipation term. This process leads to the governing equations of a viscous compressible, non-isothermal fluid flow [1, 2, 34]:

$$\partial_t \rho + \nabla \cdot (\rho \mathbf{v}) = 0, \tag{6.17}$$

$$\partial_t (\rho \mathbf{v}) + \nabla \cdot (\rho \mathbf{v} \otimes \mathbf{v} + \mathbf{J}_\mathbf{v} + \mathbf{P}^K) = \rho \mathbf{g}, \tag{6.18}$$

$$\partial_t (\rho u) + \nabla \cdot (\rho e \mathbf{v} + \mathbf{J}_q) + \mathbf{S} : \nabla \mathbf{v} = 0, \tag{6.19}$$

where u denotes the internal energy per unit mass and $\mathbf{g}$ is the gravity force/mass, $\mathbf{J}_\mathbf{v}$ includes the thermodynamic pressure and viscous stress tensors while $\mathbf{J}_q$ is the heat flux:

$$\mathbf{J}_\mathbf{v} = \left[p + \left(\frac{2}{3}\eta - \kappa \right) (\nabla \cdot \mathbf{v}) \right] \mathbf{I} - \eta (\nabla \mathbf{v} + \nabla \mathbf{v}^+), \tag{6.20}$$

$$\mathbf{J}_q = -k \nabla T, \tag{6.21}$$

with η and κ denoting the fluid and bulk viscosities, respectively, and k the thermal conductivity, all known functions of density. These equations, coupled to the van der Waals equation of state and appropriate boundary and initial conditions, yield a well-posed problem.

7. Simulation results for incompressible binary mixtures

In this Section, we review both previously published and some new results on the isothermal mixing and demixing process as well as on heat transfer enhancement due to phase separation of incompressible regular binary mixtures.

Since at this stage we are interested in qualitative results, we restrict our analysis to two-dimensional systems, so that the velocity $\mathbf{v}$ can be expressed in terms of a stream function ψ, i.e. $v_x = \partial\psi/\partial y$ and $v_y = -\partial\psi/\partial x$. Consequently, the equations of motion (6.1) and (6.13) become:

$$\frac{\partial \phi}{\partial t} = \nabla\psi \times \nabla\phi - \nabla \cdot \mathbf{J}_\phi, \tag{7.1}$$

$$\eta \nabla^4 \psi = \left(\frac{\rho R T}{M_w} \right) \nabla\tilde{\mu} \times \nabla\phi, \tag{7.2}$$

where

$$\mathbf{A} \times \mathbf{B} = A_x B_y - A_y B_x. \tag{7.3}$$

Since material transport here is diffusion-limited, the length scale of the process is the microscopic length a. Therefore, using the scaling,

$$\tilde{\mathbf{r}} = \frac{1}{a}\mathbf{r}, \quad \tilde{t} = \frac{D}{a^2} t, \quad \tilde{\psi} = \frac{1}{D N_{Pe}} \psi, \tag{7.4}$$

the equations of motion become [61, 62]:

$$\partial\phi/\partial\tilde{t} = N_{Pe} \tilde{\nabla}\tilde{\psi} \times \tilde{\nabla}\phi + \tilde{\nabla} \cdot \left\{ \tilde{\nabla}\phi - \phi(1-\phi) \left[2\Psi + \tilde{\nabla}^2 \right] \tilde{\nabla}\phi \right\}, \tag{7.5}$$

$$\tilde{\nabla}^4 \tilde{\psi} = -\tilde{\nabla}\tilde{\nabla}^2\phi \times \tilde{\nabla}\phi, \tag{7.6}$$

where N_{Pe} is the capillary Peclet number defined in (6.14). As noted by [26], Eq. (7.6) can be seen as a "static" constraint on the stream function field $\tilde{\psi}$, i.e. $\tilde{\psi} = \tilde{\psi}(\phi)$, so that the $\tilde{\psi}$-dependence on the right hand side of (7.5) can be formally dropped. Therefore, the Fourier-transformed system (7.5)-(7.6) can be written in the form

$$\frac{d}{dt}(e^{k^2 t}\hat{\phi}_{\mathbf{k}}) = e^{k^2 t}\hat{F}_{\mathbf{k}}, \tag{7.7}$$

where $\hat{\phi}_{\mathbf{k}}$ is the Fourier transform of ϕ, while the right-hand side represents the Fourier transform, $\hat{F}_{\mathbf{k}}$, of the nonlinear term of Eq. (7.5) multiplied by the integrating factor $e^{k^2 t}$. Note that the integrating factor allows the exact treatment of the diffusive term in Eq. (7.5). This system of differential equations can be time-integrated on a square domain using either the finite difference scheme described in Vladimirova *et al.* [63] or the *ad hoc* pseudo-spectral method described in Lamorgese & Mauri [26, 27, 28]. In this latter case, the nonlinear term on the right hand side of Eq. (7.6) would normally require five FFTs for its pseudospectral evaluation. However, using the identity

$$\nabla\phi \times \nabla\nabla^2\phi = \partial^2_{xy}(\phi_x^2 - \phi_y^2) + (\partial_y^2 - \partial_x^2)\phi_x\phi_y, \tag{7.8}$$

its computation requires only four FFTs. As a result, it is easy to see that each time step (e.g. assuming a simple Eulerian scheme) in (7.6) requires the evaluation of at least thirteen FFTs.

7.1. Mixing of regular mixtures

In this Section we present the simulation results of the mixing process that a viscous and macroscopically quiescent binary mixture undergoes when it is instantaneously brought from the two- to the one-phase region of its phase diagram. In addition to presenting some new data, we will also summarize the main results by Vladimirova & Mauri [64] and Lamorgese & Mauri [28].

First, let us describe the mixing process between two fluids which are initially quiescent and separated by a plane interface. In this case, the RHS of Eq. (7.6), i.e. the Korteweg body force, is identically zero, so that $\mathbf{v} = 0$ and therefore the process does not depend on the capillary Peclet number, N_{Pe}. In fact, Eq. (7.5) (in its dimensional form) is well approximated by the diffusion equation:

$$\frac{\partial\phi}{\partial t} = D^*\frac{\partial^2\phi}{\partial r_1^2}, \quad \text{with } D^* = D[1 - 2\Psi\bar{\phi}(1-\bar{\phi})], \tag{7.9}$$

where $\bar{\phi}$ represents the mean value of ϕ, as the neglected terms play a role only at the very beginning of the mixing process, when the interface is still sharp. As the results of our simulations [28] are in perfect agreement with the similarity solution resulting from Eq. (7.9), we may conclude that the mixing process of two fluids separated by an initially plane sharp interface remains one-dimensional, does not depend on N_{Pe} and is a purely diffusive process, with an effective diffusivity D^* that depends on the thermodynamic properties of the mixture, such as the Margules parameter. The same result is obtained whenever the initial configuration is one-dimensional, as in the case of an isolated drop.

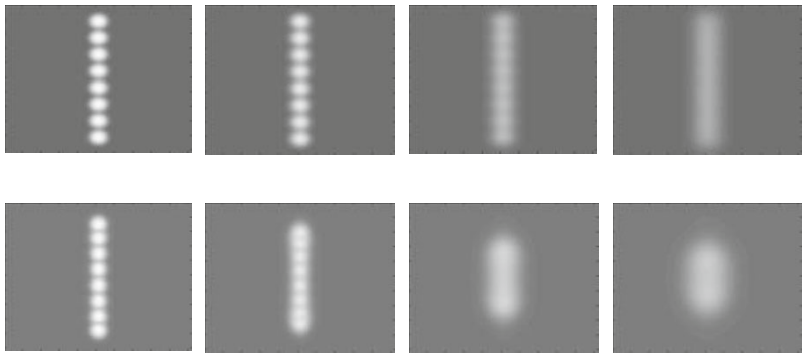

FIGURE 5. Evolution of eight identical drops with $\Psi = 1.9$ placed on a straight line at nondimensional times $t = 0.01$, 0.02, 0.04, 0.1 with $N_{Pe} = 0$ (top) vs. $N_{Pe} = 10^3$ (bottom).

When we simulate the mixing process of a collection of drops immersed in a background field, it was shown [61] that, while a single drop remains still as it is absorbed, two drops tend to attract each other and even coalesce, provided that the capillary Peclet number is large enough and the drops are initially very close to each other. This effect is further investigated in the simulations shown in Figure 5, representing the evolution of eight identical spherical drops with radius $2a$, that are placed within a quiescent bulk fluid with $\Psi = 1.9$, at distance $2a$ from each other. When $N_{Pe} = 0$, the drops do not move while they are reabsorbed by diffusion; on the other hand, when $N_{Pe} = 10^3$ they rapidly coalesce and form a larger isolated single drop. This larger drop, though, has to be eventually reabsorbed by diffusion and, being larger than the original drops, will take approximately eight times as long to disappear. This result is confirmed by simulating the mixing process of a random distribution of 250 drops with radii between $5a$ and $20a$, immersed in a quiescent continuous bulk fluid with $\Psi = 1.9$. The results of these simulations can be effectively represented in terms of the degree of mixing δ_m,

$$\delta_m(t) = \frac{\langle |\phi(\mathbf{r},t) - \phi_{av}|^2 \rangle}{\langle |\phi_0(\mathbf{r}) - \phi_{av}|^2 \rangle}. \tag{7.10}$$

This reveals that δ_m decays exponentially as $\delta_m = \exp\left(-10^3 (Dt)/(a^2\tau)\right)$, where τ is a non-dimensional decay time, with $\tau = 0.8$ when $N_{Pe} = 0$ and $\tau = 2.1$ when $N_{Pe} = 10^4$. In fact, in low-viscosity liquid systems, the Korteweg stresses initially induce a strong material flux (i.e. much larger than that due to pure molecular diffusion), thus enhancing coalescence and forming larger drops. At the end, however, as the Korteweg stresses tend to vanish, these larger drops will dissolve by diffusion only, so that the mixing process will be very slow. Therefore, we may conclude that, contrary to common thinking, in the absence of any external agitation, mixing is faster as the viscosity of the liquids increases.

Incidentally, we note here that the movement of isolated drops during phase transition has been observed experimentally by Molin *et al.* [39] and Poesio *et al.* [45], in good agreement with the predictions by Vladimirova *et al.* [61].

7.2. Spinodal decomposition of regular mixtures

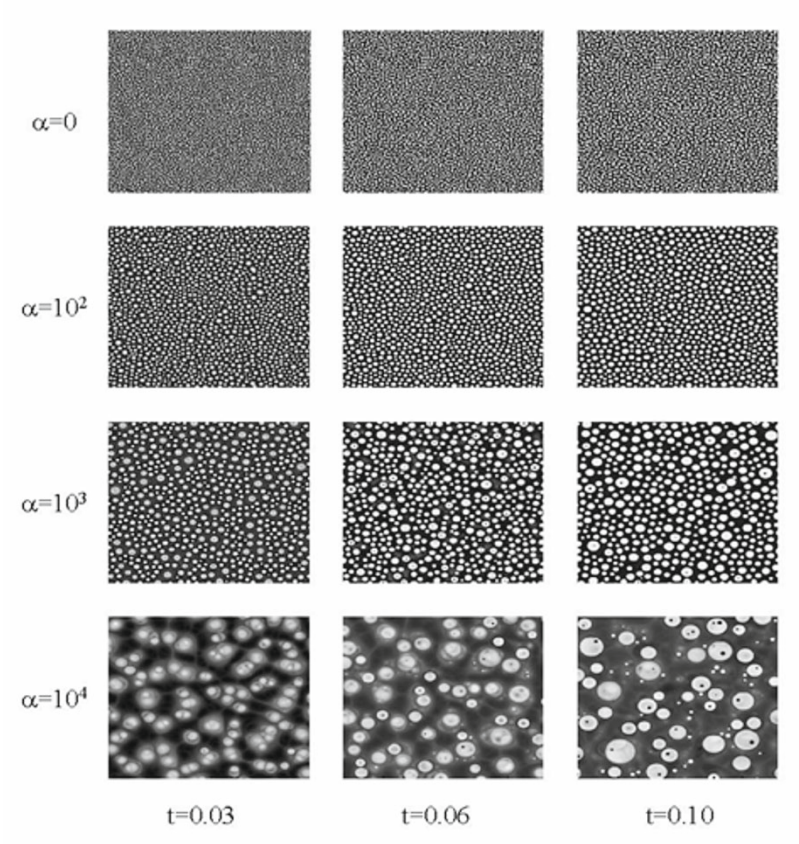

FIGURE 6. Phase separation patterns of four off-critical binary mixtures with mean composition $\phi_0 = 0.45$, Margules parameter $\Psi = 2.1$ and capillary Peclet numbers $N_{Pe} = 0, 10^2, 10^3$ and 10^4 at different non-dimensional times Dt/a^2.

In this Section we present the simulation results of Lamorgese & Mauri [26, 29] about the spinodal decomposition process that a viscous and macroscopically quiescent binary mixture undergoes when it is instantaneously brought from the one- to the two-phase region of its phase diagram, deep within the spinodal region. In Figure 6 we show some typical patterns of the spinodal decomposition process of slightly off-critical mixtures having uniform initial composition $\phi_0 = 0.45$ and for different values of N_{Pe}, when they are instantaneously quenched well below their critical temperature, i.e. with $\Psi = 2.1$. We chose this particular value of Ψ because

that is the Margules parameter of the water-acetonitrile-toluene mixture at $20°C$ that we used in our own experimental work [17, 18, 53, 7, 46]. The first row of images represents the results for $N_{Pe} = 0$, i.e. for the case when diffusion is the only mechanism of mass transfer, showing that, soon after the first drops appear, they coalesce into drop-like structures (in the critical case, we observe dendritic structures, instead). The mean composition within (and without) these structures changes rapidly, as at time $t = 0.03$ we already see two clearly distinguishable phases with almost uniform concentrations equal to 0.59 and 0.41, while at equilibrium their respective compositions are $\phi^{\alpha}_{eq} = 0.685$ and $\phi^{\beta}_{eq} = 0.315$. After this early stage, the structures start to grow, increasing their thickness and reducing the total interface area, while at the same time the composition within the domains approaches its equilibrium value. This, however, is a slow process, driven only by diffusion, and at time $t = 0.1$ the phase domains still have a drop-like geometry with a characteristic size which is just about twice as large as its value at $t = 0.01$. In the following, we will denote these slow-changing configurations as metastable states, referring to [60] for further information on their evolution. For non-zero convection, these structures thicken faster, but up to $N_{Pe} \approx 10^3$ domain growth still follows the same pattern as for $N_{Pe} = 0$: first, single-phase domains start to appear, separated from each other by sharp interfaces, and only later these structures start to grow, with increasing growth rate for larger N_{Pe}. When $N_{Pe} > 10^3$, however, phase separation occurs simultaneously with the growth process. For example, when $N_{Pe} = 10^4$, we see the formation of isolated drops of both phases, surrounded by the bulk of the fluid mixture, which is still not separated. In addition, drops appear to move fast and randomly while they grow, absorbing material from the bulk, colliding with each other and coalescing, so that they grow much faster than when molecular diffusion is the only transport mechanism. Clearly, since the motion of the interface is too quick for the diffusion of concentration to establish a metastable state within the microdomains, double, or multiple, phase separation is observed, in agreement with previous numerical [23, 57, 62] and experimental [56, 18] results. As a quantitative characterization of the influence of the convection parameter N_{Pe} on the average phase composition within the phase domains, we defined the separation depth, s, measuring the "distance" of the single-phase domains from their equilibrium state, i.e.,

$$s = \left\langle \frac{\phi(\mathbf{r}) - \phi_0}{\phi_{eq}(\mathbf{r}) - \phi_0} \right\rangle, \tag{7.11}$$

where ϕ_0 is the initial composition, and the bracket indicates volume and ensemble average. Here, ϕ_{eq} is the composition of the two phases at equilibrium, i.e.,

$$\phi_{eq}(\mathbf{r}) = \begin{cases} \phi^{\alpha}_{eq} & \text{when } \phi(\mathbf{r}) > \phi_0, \\ \phi^{\beta}_{eq} & \text{when } \phi(\mathbf{r}) < \phi_0, \end{cases} \tag{7.12}$$

where, in our simulation, $\phi^{\alpha}_{eq} = 0.685$ and $\phi^{\beta}_{eq} = 0.315$.

When the separation depth s is plotted as a function of time, we see that phase separation takes place in two different ways, depending on whether $N_{Pe} < 10^3$ or

$N_{Pe} > 10^3$. For smaller N_{Pe}, single-phase domains develop very rapidly, until they appear to be separated by sharp interfaces. From that point on, separation proceeds much more slowly, as the concentration gradients within the single-phase domains are very small, while the concentrations of the two phases across any interface change only slowly in time, asymptotically approaching quasi-equilibrium with $s = 1$. On the other hand, for $N_{Pe} > 10^3$, the growth of the separation depth is more gradual, revealing that separation and growth occur simultaneously, although obviously, at some later stage, sharp interfaces will eventually appear even in this case. In fact, dimensional analysis [62] shows that local equilibrium is reached when drops have reached $100\,\mu m$ sizes, when they start sedimenting. Consequently, the system becomes gravity driven and rapidly separates before reaching the scaling regime (i.e. when $s = 1$), so that local equilibrium is very rarely achieved for low-viscosity liquid mixtures.

Next, we studied the rate of coarsening as reflected in the growth law for the integral scale $\mathcal{L}$,

$$\mathcal{L}(t) = \frac{1}{\phi_{rms}^2} \sum_{\mathbf{k}} \frac{\langle |\hat{\tilde{\phi}}_{\mathbf{k}}|^2 \rangle}{|\mathbf{k}|}, \tag{7.13}$$

where $\tilde{\phi} = \phi - \phi_0$, ϕ_{rms} is the root-mean-squared value of ϕ, hats denote Fourier transforms, while the brackets denote averaging over a shell in Fourier space at fixed $k = |\mathbf{k}|$. As shown in Lamorgese & Mauri [26], the typical drop size $\mathcal{L}(t)$ grows linearly in time during the first stage of the process, i.e. until sharp interfaces are formed, while during the last stage it grows like $t^{1/3}$.

Note that the behavior of a phase-separating system depends as much on the driving force $\mathbf{F}_K$ as on N_{Pe}, as $\mathbf{F}_K$ (which is a function of the separation depth) can induce a strong convection only for systems with small viscosities (i.e. large N_{Pe}'s), while for very viscous systems it has hardly any effect. Very similar results were obtained by Vladimirova *et al.*[62], who used the same model but a very different numerical scheme (i.e. finite difference instead of pseudo-spectral). As shown by Lamorgese & Mauri [29], comparison between 2D and 3D results reveals that 2D simulations capture, even quantitatively, the main features of the phenomenon.

7.3. Homogeneous nucleation of regular mixtures

In thermodynamics [52], an equilibrium state (i.e. one that does not change in time while the system is isolated) is stable when it can be altered to a different state only by perturbations that do leave net effects in the environment of the system, e.g. when its temperature is changed. On the other hand, states of unstable and metastable equilibrium are equilibrium states that may be changed to different states by means of perturbations that leave no net effects on the environment. Depending on whether such perturbations are infinitesimal or finite, the system is in a state of unstable or metastable equilibrium, respectively. As we saw in Section 2, in the case of a partially miscible binary mixture the boundary of the region of stable equilibrium defines the miscibility curve in the temperature - mole fraction phase diagram $T - \phi$ at constant pressure. In addition, as an unstable system will transform spontaneously to its more

stable state, [15] showed that in those conditions the molar Gibbs free energy g of the binary mixture must be a concave function of ϕ, i.e. $\partial^2 g(T,P)/\partial\phi^2 < 0$. In particular, the boundary of the unstable region is defined by the locus $\partial^2 g(T,P)/\partial\phi^2 = 0$, which is called the spinodal curve. Therefore, the points on the phase diagram comprised between the miscibility and the spinodal curves define the metastable region. In his classical treatment on stability, Gibbs distinguished two types of perturbations that can be applied to a homogeneous system: the first is small in intensity but large in extent, as exemplified by a small composition fluctuation spread over a large volume, while the second is large in intensity but small in extent, as it happens in a nucleation process. An unstable system is best studied assuming that it is perturbed through a delocalized, infinitesimal fluctuation in composition. In this case, in fact, the problem can be linearized, showing that the intensity of any mode whose wavelength is larger than a critical value grows exponentially in time, with the maximum growth corresponding to the typical length scale of the phase separation process. Now, at this point it would seem logical to study metastable systems by perturbing them with delocalized, although finite, composition fluctuations, so that their behavior could be easily compared with that of unstable systems. Instead, Gibbs chose to use the other type of perturbation, which is large in intensity but small in extent, assuming that a uniform droplet of the minority phase would appear within the majority phase. In this way, using the concept of surface tension between two phases at thermodynamic equilibrium that he had developed, Gibbs was able to show that while, predictably, any nucleus, even an infinitesimal one, would grow spontaneously when the mixture is unstable, metastable systems become unstable only when the nucleus exceeds a critical size. Now, apart from the fact that, as Gibbs himself recognized, it is not very reasonable to assume that a small nucleus could be homogeneous, there is not a good reason today why we should study unstable and metastable systems using different procedures. In fact, Lamorgese & Mauri [27] studied non-stable binary mixtures, both unstable and metastable, by perturbing them with delocalized random fluctuations. Although this idea is not new (see the review article by Gunton [16] and references therein), they were the first to show that, as the mixture composition approaches its value at the coexistence curve, the intensity of the perturbation that is needed to trigger the instability grows exponentially. In fact, using a pseudo-spectral method, they simulated the nucleation process, showing that the metastability of the system can be characterized through either a critical radius, as in Gibbs' treatment, or the (finite) intensity of a white noise superposed on the initial uniform concentration field; this critical intensity grows exponentially as the mean composition of the mixture approaches its equilibrium value. In addition, they showed that, in general, the value of the critical radius decreases as the number density of the nucleating drops becomes very large, so that nuclei have the chance to coalesce and grow before being reabsorbed.

7.4. Effect of phase separation on heat transfer

The effect of temperature on phase separation has not been studied very carefully so far, with the exception of spinodal decomposition of very viscous mixtures, where

convection can be neglected and, therefore, the temperature field is not coupled to the velocity and concentration fields. In that case, Vladimirova *et al.* [60] showed that, as expected, the mixture starts to separate within the region where the temperature has crossed the miscibility curve. In addition, critical mixtures show a wall effect, i.e. the dendrites tend to align along the temperature gradient, while in the absence of temperature gradients they have random directions. The most interesting case, though, is that of low-viscosity, regular mixtures, where the process is convection-driven. In that case, considering that $\Psi = 2T_c/T$ and $a = \hat{a}\sqrt{\Psi}$, where $\hat{a}$ is a constant independent of T, Eqs. (6.1), (6.2) and (6.3) become:

$$\frac{\partial \phi}{\partial t} = N_{Pe}\tilde{\nabla}\tilde{\psi} \times \tilde{\nabla}\phi + \tilde{\nabla} \cdot \{\tilde{\nabla}\phi - \phi(1-\phi)[\Psi(2+\tilde{\nabla}^2)\tilde{\nabla}\phi + (2\phi - 1)\tilde{\nabla}\Psi]\}, \quad (7.14)$$

$$\tilde{\nabla}^4\tilde{\psi} = -\tilde{\nabla}(\Psi\tilde{\nabla}^2\phi) \times \tilde{\nabla}\phi, \quad (7.15)$$

$$\frac{\partial \Psi}{\partial t} = -N_{Pe}\tilde{\nabla}\tilde{\psi} \times \tilde{\nabla}\Psi + N_{Le}[\tilde{\nabla}^2\Psi - \frac{2}{\Psi}(\tilde{\nabla}\Psi)^2], \quad (7.16)$$

where we have used the scaling (7.4), with $\hat{a}$ replacing a and N_{Le} denotes the Lewis number, $N_{Le} = \alpha/D$. In Eq. (7.16) we have neglected the heat transport induced by mass diffusion and the heat generation term of the general energy conservation equation, assuming that the non-dimensional specific heat is very large, i.e., $\hat{c} = cM_W/R \gg 1$.

This case was studied by Molin & Mauri [38], showing how the temperature field is coupled to the velocity field. In all cases, the mixture starts to phase separate at the walls; then, as heat losses penetrate deeper within the domain, demixing takes place everywhere, until, at steady state, the temperature of the mixture reaches its equilibrium value. In addition, a) the mixture phase separates through the formation of bicontinuous structures; b) in the presence of convection, i.e. when $N_{Pe} = 10^2$, warm fluid tends to move towards the wall, thus enhancing heat transport.

The most obvious way to describe the heat transfer enhancement is through the Nusselt number, which is defined as the ratio between the heat flux J_q at the wall and the heat flux that one would have in the absence of convection, $(J_q)_{N_{Pe}=0}$, i.e.,

$$N_{Nu} = J_q / (J_q)_{N_{Pe}=0}. \quad (7.17)$$

Although N_{Nu} would seem to be a function of time, we saw that it actually remains almost constant and therefore can be used effectively to characterize the enhancement of heat transport due to phase transition. The most important result of our simulation was to determine how such heat transport enhancement depends on the characteristics of the process, namely the capillary Peclet and Lewis numbers, the specific heat and the quenching depth. In particular, in Figure 7 we see that heat transport increases monotonically with N_{Pe} until it reaches a plateau at $N_{Nu} \approx 2.0$ when $N_{Pe} \approx 10^6$. This result is in qualitative agreement with the experimental data by Poesio *et al.* [47].

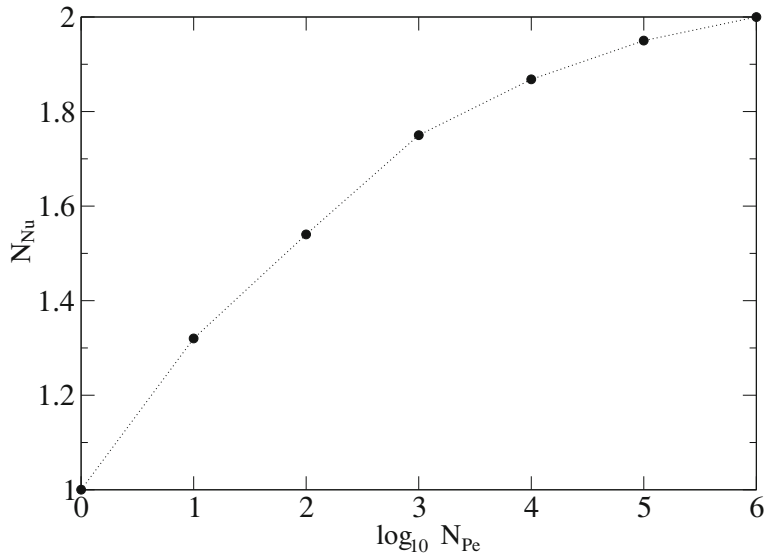

FIGURE 7. The Nusselt number, N_{Nu}, as a function of the Peclet number, N_{Pe}, when $N_{Le} = 1$ and with no source term.

8. Spinodal decomposition of a van der Waals fluid

We discuss below the simulation results obtained by Lamorgese & Mauri [30] on the isothermal liquid-vapor spinodal decomposition of a van der Waals fluid, occurring after quenching it instantaneously from a single-phase equilibrium state to the unsteady two-phase region of its phase diagram.

The governing equations (see Section 6.2) were made dimensionless based on both a diffusive scaling, which is relevant only at the beginning of phase separation, and an acoustic, or convective, scaling, which is relevant at the late stage of phase separation. In particular, in the acoustic scaling, defining a reference speed of sound, $u_s = (RT_C/M_W)^{1/2}$, we set:

$$\tilde{\mathbf{x}} = \frac{\mathbf{x}}{L}, \quad \tilde{t} = \frac{u_s t}{L}, \quad \tilde{\mathbf{u}} = \frac{\mathbf{u}}{u_s}, \quad N_{Re} = \frac{\rho_c u_s a}{\eta_I}, \tag{8.1}$$

$$\tilde{\rho} = \frac{\rho}{\rho_C}, \quad \tilde{p} = \frac{p}{p_C^*}, \quad \tilde{T} = \frac{T}{T_C}. \tag{8.2}$$

where η_I is the viscosity of the liquid phase, $\tilde{\rho}$, $\tilde{p}$ and $\tilde{T}$ are reduced density, pressure and temperature, respectively, as ρ_C and T_C are the critical density and temperature, while $p_C^* = \rho_C RT_C/M_W$ is the critical pressure if the fluid were a perfect gas (R and M_W being the gas constant and the molecular weight). In addition, without loss of generality, we assume that $\beta = N_A d^3 \rho_C/M_W = 1$, where d and N_A denote a molecular diameter and the Avogadro number, respectively. Here, N_{Re} is a capillary Reynolds number, which plays a very similar role as the capillary Peclet number, N_{Pe}, in the incompressible binary mixture case.

In the governing equations, all external forces, and buoyancy in particular, were assumed to be negligible, which amounts to assuming that the Bond number is very small. In other words, drop and bubble sizes ℓ are small compared to the capillary length, i.e., $\ell \ll \sqrt{\sigma/g\,(\rho_I - \rho_{II})}$ (with σ the surface tension, g the gravity field and with I and II denoting the liquid and vapor phases at equilibrium).

The problem was discretized using a structured, staggered arrangement of the conserved variables [40, 41], with spatial derivatives computed via sixth-order compact finite differences [32]. Temporal advancement was effected via a third-order Runge-Kutta scheme. The simulations were conducted at $\tilde{T} = 0.9$, for different values of N_{Re}, assuming an infinite expanse of fluid (modeled via periodic boundary conditions). At this temperature, a representative vapor-liquid viscosity ratio was chosen to be $r = 10^{-3}$. Initially, we assumed quiescent conditions with a density field being the sum of a Gaussian white noise superposed on a uniform constant density $\rho = \rho_0$. We chose values of $\tilde{\rho}_0 = 0.7$, 1.042, 1.3 in the spinodal range, i.e., $\tilde{\rho}_0 \in [\tilde{\rho}_s^{II}, \tilde{\rho}_s^{I}]$, where $\tilde{\rho}_s^{I} = 1.39$ and $\tilde{\rho}_s^{II} = 0.654$ denote the liquid and vapor spinodal densities at the given temperature. (For a van der Waals fluid these values are easily found by solving the algebraic relation $\tilde{\rho}(3 - \tilde{\rho})^2 = 4\tilde{T}$.) Specifically, $\tilde{\rho}_0 = 1.042$ is the critical density, while $\tilde{\rho}_0 = 0.7$ and $\tilde{\rho}_0 = 1.3$ correspond to the densities of the vapor-rich and liquid-rich mixtures at equilibrium, respectively.

As expected, we observed [30] that the phase-ordering process after the critical quench $\tilde{\rho}_0 = 1.042$ is characterized by the formation of bicontinuous structures, which subsequently grow and coalesce. For the off-critical quench, $\tilde{\rho}_0 = 1.3$, instead, as we see in Fig. 8, the phase separation pattern consists of a random collection of rapidly coalescing nuclei of the minority phase, surrounded by the majority phase. Only after the first spinodal pattern is formed (i.e. a bicontinuous pattern for the critical quench, or a random collection of nuclei for the off-critical quench), do the single-phase domains start to grow and coalesce, at an increasing rate for larger capillary Reynolds number, N_{Re}.

As a quantitative characterization of the influence of the convection parameter N_{Re} on the average phase composition of the two-phase fluid, we defined the separation depth, s, through Eqs. (7.11)-(7.12), with the density ρ replacing the concentration ϕ, measuring the "distance" of the single-phase domains from their equilibrium state, i.e.,

$$s = \left\langle \frac{\rho(\boldsymbol{x}) - \rho_0}{\rho_{eq}(\boldsymbol{x}) - \rho_0} \right\rangle, \tag{8.3}$$

where ρ_0 is the initial mean density, and the brackets indicate volume and ensemble averaging. Here, ρ_{eq} denotes the steady-state density of the liquid phase, ρ_I, or of the vapor phase, ρ_{II}, depending on the local density $\rho(\boldsymbol{x})$.

Figure 9 shows the temporal evolution of the separation depth for $N_{Re} =$ 1, 10, 100, 1000. The solid curves in this figure were obtained from 2D simulations on a 256^2 grid, while the dotted lines are from 3D simulations on a 128^3 grid, showing remarkable quantitative agreement. Here, after a time delay, with no detectable liquid-vapor phase separation, first the system reaches local equilibrium (with the formation of nuclei having sharp interfaces), and then these nuclei start to grow,

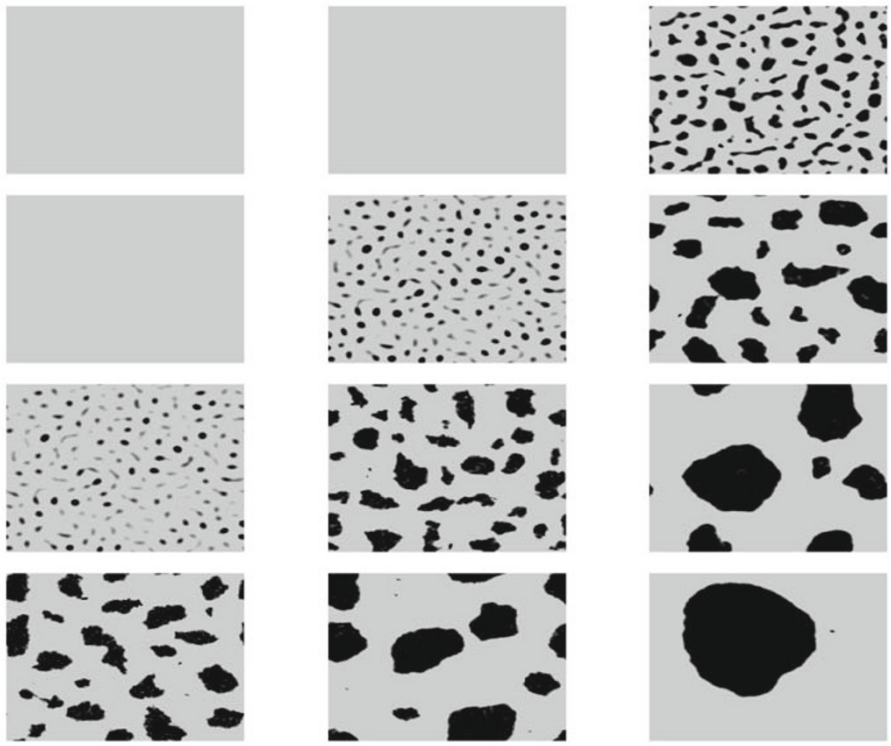

FIGURE 8. Liquid-vapor spinodal decomposition of an off-critical van der Waals fluid (with $\tilde{\rho}_0 = 1.3$) at different non-dimensional times (diffusive scaling) $\tilde{t} = 3\,10^{-3}$, 10^{-2} and $5\,10^{-2}$, with $N_{Re} = 1$, 10, 10^2 and 10^3 from top to bottom.

even at large N_{Re}. This is in contrast with phase separation in viscous liquid binary mixtures, where for large N_{Pe} the two events occur simultaneously (cf. discussion in Section 7.2), and in any case local equilibrium is reached only very late in the process, well after the appearance of nuclei with sharp interfaces.

Next, we studied the rate of coarsening as reflected in the growth law for the integral scale (7.13),

$$\mathcal{L}(t) = \frac{1}{\rho_{rms}^2} \sum_{\mathbf{k}} \frac{\langle |\hat{\tilde{\rho}}_{\mathbf{k}}|^2 \rangle}{|\mathbf{k}|}, \tag{8.4}$$

where $\tilde{\rho} = \rho - \langle \rho \rangle$, ρ_{rms} is the root-mean-squared value of ρ, hats denote Fourier transforms, while the brackets denote averaging over a shell in Fourier space at fixed $k = |\mathbf{k}|$. As can be seen in Fig. 10, after an initial stage that strongly depends on the initial conditions, then sharp interfaces are formed and domains stop growing, concomitant to their composition rapidly reaching local equilibrium. At this point, during the latest stage, growth is driven by inertial forces and is characterized by a $\frac{2}{3}$ power-law behavior, in agreement with predictions based on simple dimensional analysis [55, 14].

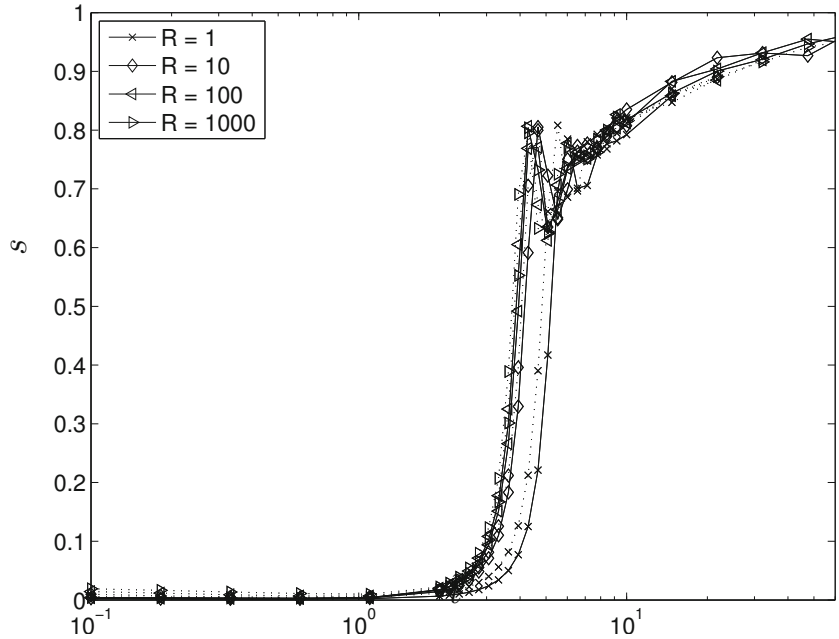

FIGURE 9. Separation depth vs. time (acoustic scaling) for different values of $N_{Re} = 1$, 10, 100, 1000 from 2D simulations with $\tilde{\rho}_0 = 1.3$ (solid) vs. 3D simulation results (dotted).

9. Conclusions

The main message of this review article is that we need to include intermolecular interactions in the classical hydrodynamic theory whenever we are interested in phenomena whose length scale is comparable to the interface thickness. This happens in the theory of contact line motion, the fluid mechanics of microdevices, as well as in the mixing and demixing of partially miscible mixtures that have been outlined here. In all these cases, the final objective is that of determining, through a "correct" microscopic description, the appropriate boundary conditions of the classical equations of fluid dynamics that are applicable to macroscopic domains. The diffuse interface method, in particular, provides a sound theoretical basis for studying mixing and de-mixing of fluid systems. Here, we have reviewed its basic theoretical foundations for both pure fluids and binary mixtures, above all when each component behaves like a van der Waals fluid. We saw that the basic difference between the diffuse interface formulation and the classical approach is the presence of a capillary, or Korteweg, stress tensor in the momentum balance, expressing the tendency of the system to minimize its free energy. This extra stress gives rise to a body force, which is proportional to the gradient of the chemical potential difference, inducing a convection that, during phase transition, is much larger than that due to pure molecular diffusion. As it is identically zero at equilibrium, this force can be thought of as a non-equilibrium capillary force, whose net effect is

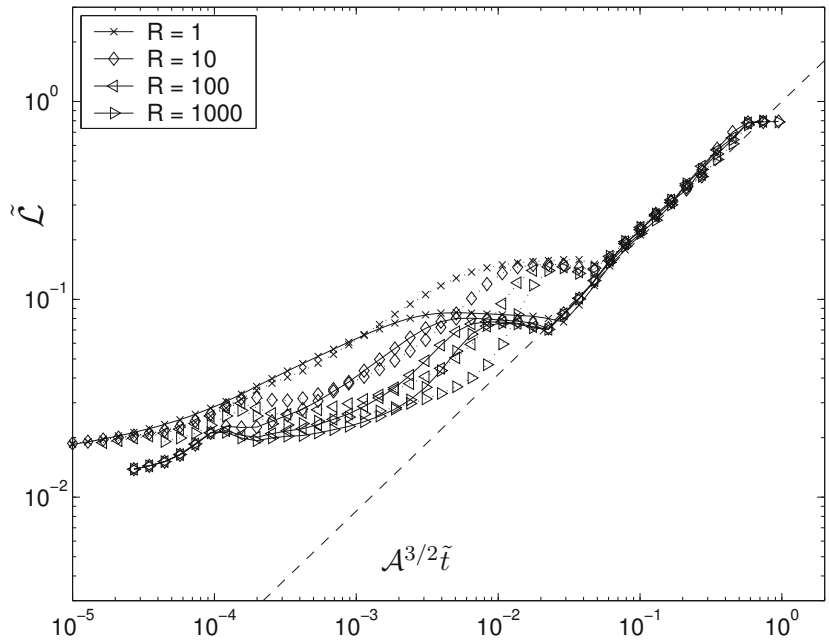

FIGURE 10. Integral scale vs. time (acoustic scaling) for different values of $N_{Re} = 1$, 10, 100, 1000 from 2D simulations with $\tilde{\rho}_0 = 1.3$ (solid) vs. 3D simulation results (dotted). $\mathcal{A}$ is the non-dimensional $(\sigma/\rho)^{1/3}$ ratio, based on the scaling theory growth law $\tilde{\mathcal{L}} = \mathcal{A}\tilde{t}^{2/3}$.

that of generating an attractive force between domains of the same phase. Accordingly, coalescence is greatly enhanced in out-of-equilibrium, low viscosity mixtures, when convection-induced fluxes become dominant over diffusion fluxes. This phenomenon is observed during the mixing process of liquid binary mixtures, where, however, once larger domains are formed, they must eventually dissolve by diffusion and, therefore, the process turns out to be actually retarded as the viscosity of the system decreases. Also, very interesting effects are observed when heat transfer is considered, as the chemical potential gradient-induced convection arising during phase transition greatly accelerates the transport of heat. Finally, we show that the influence of this convection is most clearly manifested during phase separation. In particular, when inertial forces are small, as in liquid binary mixtures, the typical growth law for the domain size R changes from $R \propto t^{1/3}$, for very viscous systems, where diffusion prevails, to $R \propto t$, for convection-driven processes, as one can easily obtain by imposing that capillary forces be balanced by viscous forces. In the case of single-component, liquid-vapor phase separation, instead, we obtain a $\frac{2}{3}$ power-law behavior, as capillary forces are balanced by inertial forces. In addition, here first the system reaches local equilibrium (with the formation of nuclei having sharp interfaces), and then these nuclei start to grow, while for viscous liquid binary mixtures the two events occur simultaneously.

These examples demonstrate that the phase field approach allows to describe, even quantitatively, phenomena, such as drop coalescence and breaking, that cannot be resolved using conventional two-phase flow models.

References

[1] D. Anderson, G. McFadden, and A. Wheeler, *Diffuse-interface methods in fluid mechanics*, Ann. Rev. Fluid Mech. **30** (1998), 139–165.

[2] L. Antanovskii, *Microscale theory of surface tension*, Phys. Rev. E **54** (1996), 6285–6290.

[3] J. Cahn, *On spinodal decomposition*, Acta Metall. Mater **9** (1961), 795–801.

[4] J. Cahn, *Critical point wetting*, J. Chem. Phys. **66** (1977), 3667–3772.

[5] J. Cahn, and J. Hilliard, *Free energy of a nonuniform system. I. Interfacial free energy*, J. Chem. Phys. **28** (1958), 258–267.

[6] J. Cahn, and J. Hilliard, *Free energy of a nonuniform system. III. Nucleation in a two-component incompressible fluid*, J. Chem. Phys. **31** (1959), 688–699.

[7] F. Califano, and R. Mauri, *Drop size evolution during the phase separation of liquid mixtures*, Ind. Eng. Chem. Res. **43** (2004), 349–353.

[8] E. Cussler, *Diffusion*, Cambridge University Press, 1982.

[9] H. Davis, and L. Scriven, *Stress and structure in fluid interfaces*, Adv. Chem. Phys. **49** (1982), 357–454.

[10] S. de Groot, and P. Mazur, *Non-Equilibrium Thermodynamics*, Dover, New York, 1984.

[11] P.G. de Gennes, *Dynamics of fluctuations and spinodal decomposition in polymer blends*, J. Chem. Phys. **72** (1980), 4756–4763.

[12] B.U. Felderhof, *Dynamics of the diffuse gas-liquid interface near the critical point*, Physica **48** (1970), 541–560.

[13] A. Frezzotti, L. Gibelli, and S. Lorenzani, *Mean field kinetic theory description of evaporation of a fluid into vacuum*, Phys. Fluids **17**, 012102 (2005).

[14] H. Furukawa, *Role of inertia in the late stage of the phase separation of a fluid*, Physica A **204** (1994), 237–245.

[15] J. Gibbs, *On the equilibrium of heterogeneous substances*, 1876; reprinted in *Scientific Papers by J. Willard Gibbs*, Vol. 1, Dover, New York (1961).

[16] J. Gunton, *Homogeneous nucleation*, J. Stat. Phys. **95** (1999), 903–923.

[17] R. Gupta, R. Mauri, and R. Shinnar, *Liquid-liquid extraction using the composition induced phase separation process*, Ind. Eng. Chem. Res. **35** (1996), 2360–2368.

[18] R. Gupta, R. Mauri, and R. Shinnar, *Phase separation of liquid mixtures in the presence of surfactants*, Ind. Eng. Chem. Res. **38** (1999), 2418–2424.

[19] J. W. Herivel, *The derivation of the equations of motion of an ideal fluid by hamilton's principle*, Proc. Cam. Phil. Soc., **51** (1955), 344–353.

[20] P.C. Hohenberg, and B.I. Halperin, *Theory of dynamic critical phenomena*, Rev. Mod. Phys. **49** (1977), 435–480.

[21] J.H. Israelachvili, *Intermolecular and Surface Forces*, Academic Press, 1992.

[22] D. Jacqmin, *Contact-line dynamics of a diffuse fluid interface*, J. Fluid Mech. **402** (2000), 57–88.

[23] D. Jasnow, and J. Viñals, *Coarse-grained description of thermo-capillary flow*, Phys. Fluids **8** (1996), 660–669.

[24] K. Kawasaki, *Kinetic equations and time correlation functions of critical fluctuations*, Ann. Phys. **61** (1970), 1–56.

[25] D. Korteweg, *Sur la forme que prennent les équations du mouvements des fluides si l'on tient compte des forces capillaires causées par des variations de densité considérables mais continues et sur la théorie de la capillarité dans l'hypothèse d'une variation continue de la densité*, Archives Néerlandaises des Sciences Exactes et Naturelles. Series II, **6** (1901), 1–24.

[26] A. Lamorgese, and R. Mauri, *Phase separation of liquid mixtures*, in Nonlinear Dynamics and Control in Process Engineering: Recent Advances, G. Continillo, S. Crescitelli, and M. Giona, eds., Springer, 2002, pp. 139–152.

[27] A. Lamorgese, and R. Mauri, *Nucleation and spinodal decomposition of liquid mixtures*, Phys. Fluids **17** (2005), 034107.

[28] A. Lamorgese, and R. Mauri, *Mixing of macroscopically quiescent liquid mixtures*, Phys. Fluids **18** (2006), 044107.

[29] A. Lamorgese, and R. Mauri, *Diffuse-interface modeling of phase segregation in liquid mixtures*, Int. J. Multiphase Flow **34** (2008), 987–995.

[30] A. Lamorgese, and R. Mauri, *Diffuse-interface modeling of liquid-vapor phase separation in a van der Waals fluid*, Phys. Fluids **21** (2009), 044107.

[31] L. Landau, and E. Lifshitz, *Statistical Physics, Part I*, Pergamon Press, 1980.

[32] S.K. Lele, *Compact finite-difference schemes with spectral-like resolution*, J. Comput. Phys. **103** (1992), 16–42.

[33] G.W.F. Von Leibnitz, *Nouveaux Essais sur l'Entendement Humain*, book II, Ch. IV., 1765. Here Leibnitz applied to the natural world the statement "Natura non facit saltus" (Nature does not jump) that in 1751 Lineus (i.e. C. von Linn) in *Philosophia Botanica*, Ch. 77, had referred to species evolution.

[34] J. Lowengrub, and L. Truskinovsky, *Quasi-incompressible Cahn-Hilliard fluids and topological transitions*, P. R. Soc. London A **454** (1998), 2617–2654.

[35] Titus Carus Lucretius, *De Rerum Natura*, Book I, 50 B.C.E. "Corpus inani distinctum, quoniam nec plenum naviter extat nec porro vacuum."

[36] R. Mauri, R. Shinnar, and G. Triantafyllou, *Spinodal decomposition in binary mixtures*, Phys. Rev. E **53** (1996), 2613–2623.

[37] J.C. Maxwell, Capillary action, 1876; reprinted in *Scientific Paper of James Clerk Maxwell,* Vol. 2, Dover, New York, 1952, pp. 541-591.

[38] D. Molin, and R. Mauri, *Enhanced heat transport during phase separation of liquid binary mixtures*, Phys. Fluids **19** (2007), 074102.

[39] D. Molin, R. Mauri, and V. Tricoli, *Experimental evidence of the motion of a single out-of-equilibrium drop*, Langmuir **23** (2007), 7459–7461.

[40] S. Nagarajan, S.K. Lele, and J.H. Ferziger, *A robust high-order compact method for large-eddy simulation*, J. Comp. Phys. **191** (2003), 392–419.

[41] S. Nagarajan, S.K. Lele, and J.H. Ferziger, *Leading-edge effects in bypass transition*, J. Fluid Mech. **572** (2007), 471–504.

[42] E. Nauman and D. He, *Nonlinear diffusion and phase separation*, Chem. Eng. Sci. **56** (2001), 1999–2018.

[43] L. Pismen, *Nonlocal diffuse interface theory of thin films and moving contact line*, Phys. Rev. E **64** (2001), 021603.

[44] L. Pismen, and Y. Pomeau, *Disjoining potential and spreading of thin liquid layers in the diffuse-interface model coupled to hydrodynamics*, Phys. Rev. E **62** (2000), 2480–2492.

[45] P. Poesio, G. Beretta, and T. Thorsen, *Dissolution of a liquid microdroplet in a nonideal liquid-liquid mixture far from thermodynamic equilibrium*, Phys. Rev. Lett. **103** (2009), 064501.

[46] P. Poesio, G. Cominardi, A. Lezzi, R. Mauri, and G. Beretta, *Effects of quenching rate and viscosity on spinodal decomposition*, Phys. Rev. E **74** (2006), 011507.

[47] P. Poesio, A. Lezzi, and G. Beretta, *Evidence of convective heat transfer enhancement induced by spinodal decomposition*, Phys. Rev. E **75** (2007), 066306.

[48] S.D. Poisson, *Nouvelle Theorie de l'Action Capillaire*, Bachelier, Paris, 1831.

[49] Lord Rayleigh, *On the theory of surface forces. II. Compressible fluids.* Philosophical Magazine **33** (1892), 209–220.

[50] C. Rohde, *On local and non-local avier-Stokes.Korteweg systems for liquid-vapour phase transition*, ZAMM **85** (2005), 839–857.

[51] J. Rowlinson, and B. Widom, *Molecular Theory of Capillarity*, Oxford University Press, 1982.

[52] I.S. Sandler, *Chemical and Engineering Thermodynamics, 3rd Ed.*, Wiley, 1999, Ch. 7.

[53] G.M. Santonicola, R. Mauri, and R. Shinnar, *Phase separation of initially non-homogeneous liquid mixtures*, Ind. Eng. Chem. Res. **40** (2001), 2004–2010.

[54] J. Serrin, *Mathematical principles of classical fluid mechanics*, in Encyclopedia of Physics, Vol. VIII-1, S. Flügge, ed., Springer, 1959, pp. 125–263.

[55] E. Siggia, *Late stages of spinodal decomposition in binary mixtures*, Phys. Rev. A **20** (1979), 595–605.

[56] H. Tanaka, *Coarsening mechanisms of droplet spinodal decomposition in binary fluid mixtures*, J. Chem. Phys. **105** (1996), 10099–10114.

[57] H. Tanaka and T. Araki, *Spontaneous double phase separation induced by rapid hydrodynamic coarsening in two-dimensional fluid mixtures*, Phys. Rev. Lett. **81** (1998), 389–392.

[58] U. Thiele, S. Madruga, and L. Frastia, *Decomposition driven interface evolution for layers of binary mixtures: I. Model derivation and stratified base states*, Phys. Fluids **19** (2007), 122106.

[59] J. van der Waals, *The thermodynamic theory of capillarity under the hypothesis of a continuous variation of density*, 1893; reprinted in *Journal of Statistical Physics*, **20** (1979), 200–244.

[60] N. Vladimirova, A. Malagoli, and R. Mauri, *Diffusion-driven phase separation of deeply quenched mixtures*, Phys. Rev. E **58** (1998), 7691–7699.

[61] N. Vladimirova, A. Malagoli, and R. Mauri, *Diffusio-phoresis of two-dimensional liquid droplets in a phase separating system*, Phys. Rev. E **60** (1999a), 2037–2044.

[62] N. Vladimirova, A. Malagoli, and R. Mauri, *Two-dimensional model of phase segregation in liquid binary mixtures*, Phys. Rev. E **60** (1999b), 6968–6977.

[63] N. Vladimirova, A. Malagoli, and R. Mauri, *Two-dimensional model of phase segregation in liquid binary mixtures with an initial concentration gradient*, Chem. Eng. Sci. **55** (2000), 6109–6118.

[64] N. Vladimirova, and R. Mauri, *Mixing of viscous liquid mixtures*, Chem. Eng. Sci. **59** (2004), 2065–2069.

Andrea G. Lamorgese
Department of Chemical Engineering
The City College of CUNY
10031 New York
U.S.A.
e-mail: lga@che.ccny.cuny.edu

Dafne Molin
Department of Mechanical Engineering
University of Brescia
Via Branze 38
25123 Brescia
Italy
e-mail: dafmolin@gmail.com

Roberto Mauri
Department of Chemical Engineering, Industrial Chemistry and Material Science
University of Pisa
Via Diotisalvi 2
56126 Pisa
Italy
e-mail: r.mauri@diccism.unipi.it

Lecture held by R. Mauri in the *Seminario Matematico e Fisico di Milano* on May 23, 2011
Received: June 27, 2011.